AMERICAN UNIVERSITY OF BEIRUT

A DFT INVESTIGATION OF THE MECHANISM OF ESTER
HYDROGENATION BY AN OCTAHEDRAL IRON-AMINO
HYDRIDE CATALYST

by
ALI DARWICH ABO TAKA

A thesis
submitted in partial fulfillment of the requirements
for the degree of Master of Science
to the Department of Chemistry
of the Faculty of Arts and Sciences
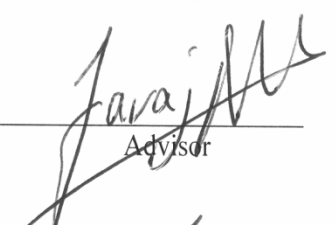at the American University of Beirut

Beirut, Lebanon
July 2016

A DFT INVESTIGATION OF THE MECHANISM OF ESTER HYDROGENATION BY AN OCTAHEDRAL IRON-AMINO HYDRIDE CATALYST
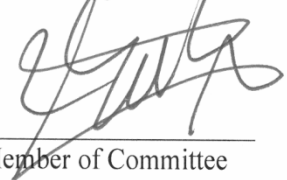
by
ALI DARWICH ABO TAKA

Approved by:

_____

Dr. Faraj Hasanayn, Professor   Advisor
Chemistry

_____

Dr. Mazen Ghoul, Professor   Member of Committee

_____

Dr. Mohamad Hmadeh, Assistant Professor   Member of Committee

Date of thesis defense: July, 2016

AMERICAN UNIVERSITY OF BEIRUT

THESIS, DISSERTATION, PROJECT RELEASE FORM

Student Name: _Abotaka_ _Ali_ _Darwish_

                 Last   First   Middle

⬤ Master's Thesis   ◯ Master's Project   ◯ Doctoral   Dissertation

☑ I authorize the American University of Beirut to: (a) reproduce hard or electronic copies of my thesis, dissertation, or project; (b) include such copies in the archives and digital repositories of the University; and (c) make freely available such copies to third parties for research or educational purposes.

☐ I authorize the American University of Beirut, to: (a) reproduce hard or electronic copies of it; (b) include such copies in the archives and digital repositories of the University; and (c) make freely available such copies to third parties for research or educational purposes
after:

One --- year from the date of submission of my thesis, dissertation, or project.
Two --- years from the date of submission of my thesis, dissertation, or project.
Three --- years from the date of submission of my thesis, dissertation, or project.

Ali Abotaka   _Feb. 7 2017_

Signature   Date

ACKNOWLEDGMENTS

AN ABSTRACT OF THE THESIS

Ali Darwich Abo Taka   for   Master of Science
                                     Major: Chemistry

Title: A DFT Investigation of the Mechanism of Ester Hydrogenation by an Octahedral Iron-Amino Hydride Catalyst.

Ester hydrogenation is an important reaction in chemistry that is currently done using stoichiometric environmentally unfriendly hydrogenation reagents such as lithium aluminum hydride. The search for more green methods based on hydrogen gas resulted in the discovery of several classes of homogeneous catalysts for this reaction. However, these catalysts are still not efficient enough for practical applications, and there is still limited understanding of the mechanism.

In this work, density functional theory (DFT) is used to investigate three fundamentally different mechanisms leading to C-OMe bond cleavage in the reaction between methyl benzoate and the octahedral hydrogenation catalyst trans-[Fe(H)2(^{i}Pr$_4$PNP)(CO)] (where PNP has an aliphatic diethyl-amine backbone). First we calculate a conventional Noyori type mechanism following two stages: (i) stepwise bifunctional hydrogenation of the carbonyl group of the ester into separated hemiacetal and an unsaturated amido complex, and (ii) C-OMe cleavage by another bifunctional reaction between the hemiacetal and the amido complex to give the octahedral trans-[Fe(H)(OMe)(^{i}Pr$_4$PNP)(CO)] and benzaldehyde. The combined two stages are equivalent to an H/OR metathesis for hydride/alkoxide exchange between an acyl group and a metal center. Second we consider two variations on a hemiacetaloxide ion-pair formation and 1,1-slippage mechanism to the same H/OR metathesis, one following direct α-H/OR slippage of the hemiacetaloxide, and another following a sequence of α-H/O- and α-O-/OR slippages that mediate, respectively, carbonyl group (ester) insertion and (aldehyde) de-insertion. When computed in a polarizable solvent continuum representing THF as solvent the two routes to H/OR metathesis is found to be competitive. However, when a methanol continuum is applied in the calculations the slippage route is greatly stabilized over hemiacetal formation. Finally, a distinct bifunctional mechanism for C-OR cleavage of the hemiacetal leading to a metal coordinated aldehyde and an alcohol is shown to be less probable than the metathesis routes.
We also investigated alternative pathway for catalyst regeneration in two different solvents, THF and methanol. As well as we studied the effect of varying the nature of the ester on the mechanism.

CONTENTS

Chapter

ILLUSTRATIONS

TABLES

CHAPTER I

INTRODUCTION

A. Historic Background for the Hydrogenation of unsaturated bonds

1. Heterogeneous Hydrogenation

Hydrogenation of unsaturated bonds, such as olefins and carbonyls, is a central reaction in chemistry and is of great importance in synthesis. Advancement in this area was done by Sabatier and Senderens. They developed a nickel-based hydrogenation process for the conversion of unsaturated organic molecules such as carbonyls and olefins.[1] Hydrogenation of such compounds was done by allowing the organic molecule vapor along with hydrogen gas to flow over a hot finely divided nickel.[2]

This process is affected by two conditions, the purity of the nickel and the temperature of the reaction.[2] For example, the presence of any small amounts of sulfur or bromine can deactivate the catalyst, as well as each of the hydrogenation processes works within a specific range of temperature. For instance, forming cyclohexane from benzene is done at temperatures ranging from 70 °C to 190 °C, increasing the temperature above 300 °C, reduction of benzene to methane takes place.[3] Besides nickel, Sabatier found that platinum, cobalt, iron and copper can catalyze the hydrogenation reactions. A general reaction scheme is represented in figure I.1.
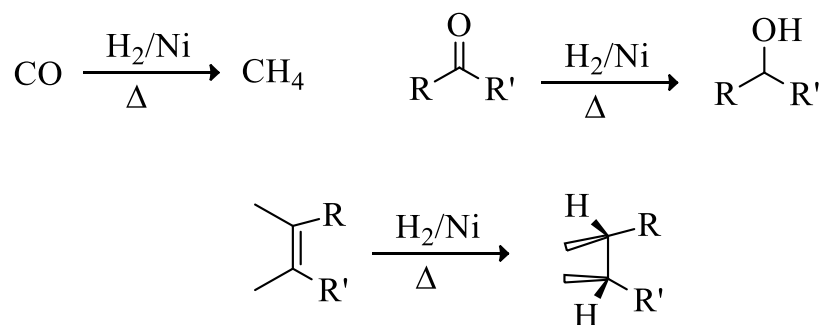
Figure I-1 General Scheme for the hydrogenation reaction

a. Olefins Hydrogenation

Homogeneous hydrogenations are usually carried out with catalysts based on Rhodium, Ruthenium, and Iridium [4-6]. These complexes are more sensitive than heterogeneous catalysts, but are more selective on the other hand. [7] Introducing the idea of homogeneous hydrogenation was a significant step in synthetic process which was also extensively studied in the area of homogenous catalysis and pioneered by Wilkinson.[8] This catalysis is done under the presence of hydrogen, or any hydrogen donors such as alcohols. [7] The advancement in this area had permitted a remarkable development in organometallic chemistry, where homogenous hydrogenation was done under mild conditions. [9] Improving Wilkinson catalyst was done by several groups such as Knowles[10] and Horner[11] ,they were the pioneers of the idea of replacing PPh_3 by a chiral phosphine (methylpropylphenylphosphine). However, they reported a low enantiomeric excess of only 15% for the hydrogenation of non-functionalized olefins. An important breakthrough in increasing the enantioselectivity was done by Kagan, he reported an enantiomeric excess of 70%. [12] Monodentate and bidentate

ligands are used in asymmetric hydrogenation in general, and a huge competition is still

going on.

b. Carbonyl Hydrogenation

After achieving the selective hydrogenation for olefins, great effort was put for

carbonyl hydrogenation. Advancement in this area was brought by Noyori, he was one

of the innovators in doing selective hydrogenation of ketones and aldehydes.[13] Early

work by Noyori achieved hydrogenation at 28 °C and 4 atm H_2 gas using 0.2 mol%

catalyst loading which are relatively mild conditions. [13] Improving the activity was

done by designing ruthenium complex containing chiral diphosphines and chiral

diamines, this design achieved enantionmeric excess up to 99%. These types of catalyst

were proposed to act in an outer-sphere bifunctional mechanism characterized by the

non-innocent behavior of the ligand. This mechanism is outlined in figure I.2. The

mechanism starts with a concerted transfer of the hydride and the proton to the carbonyl

to produce the five coordinate product (Ru=N). It was postulated that this step goes in

an outer-sphere mode passing through the formation of the six coordinate intermediate.

The octahedral ruthenium complex is regenerated by the reaction of H_2 with the five-

coordinate complex where the H_2 undergoes heterolytic cleavage at the Ru=N site. [14]
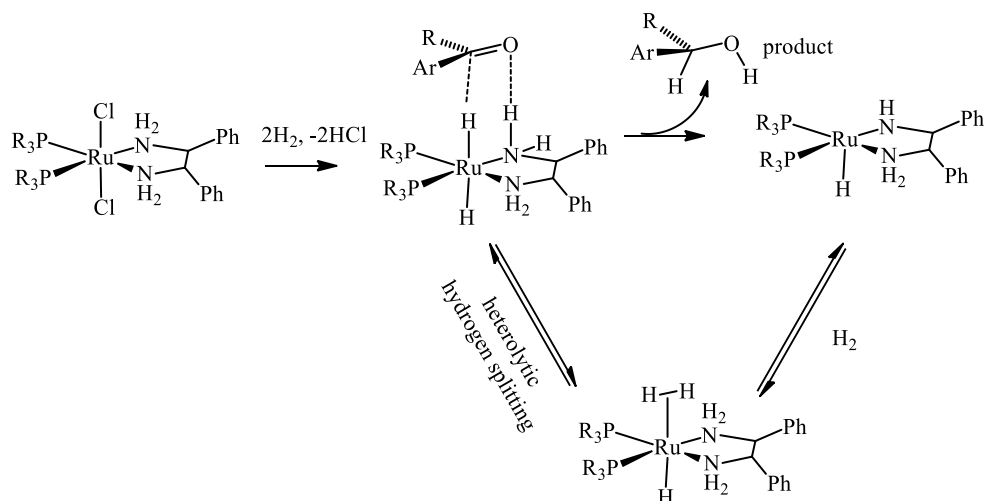
Figure I-2 Noyori's outer-sphere bifunctional concerted mechanism

B. Methods for Ester Hydrogenation

1. Heterogeneous Hydrogenation

Heterogeneous catalysis for ester hydrogenation has a long history. Adkins used Ba/Cu/Cr oxides catalysts to hydrogenate esters giving a yield of 90%. [15-17] However, this hydrogenation is done under relatively harsh conditions, where the pressure of hydrogen was 22 atmosphere and at an elevated temperature of 250 °C. [15] For industrial usage, the long stability of the catalyst is of great importance. For example, the hydrogenation of fatty acid esters suffers from catalyst deactivation at a fast rate, by the sulfur and phosphate found in bio-derived compounds. [18, 19]

The progress for finding alternative catalysts that can be more selective is really crucial. For this purpose, bimetallic catalyst had been proposed having a bifunctional nature. Early example in this domain was demonstrated by Narasimhan [20] where hydrogenation of methyl oleate to aleyl acohol (not methyl stearate or stearyl alcohol) by using Ru–Sn–B/Al$_2$O$_3$ was achieved with 62% of selectivity.

4

However, this hydrogenation is done under 44 bar H_2 pressure and at 270 °C. It was proposed that the role of B is to enhance electron density of surface Ru, and the presence of tin was important for the dispersion of metallic ruthenium.

Developing ruthenium bimetallic system was done by Li's group. Li designed the Ru-Pt/AlOOH catalyst [21] that was efficient in the hydrogenation of methyl propionate in aqueous mediums. This process was done at a relatively lower temperature than the past catalyst (180 °C) and obtained a 90% conversion with 98% selectivity for 1-propanol. This enhancement was attributed to the hydrogen bonding between the substrate and the hydroxyl groups including water that facilitated the hydrogenation of the esters.

Besides ruthenium, the usage of coinage bimetallic catalysts such as silver-gold catalyst, showed a high efficient conversion at low temperature compared to the previous one (145 °C). The improvement in this activity is divided between the facilitation of the interaction with hydrogen gas by silver, and the strong affinity for gold with the carbonyl group.[22]

2. *Hydride Reducing Agents*

Hydrogenation of carbonic and carboxylic acid derivatives using homogenous catalysts are also important in synthesis; however, they cannot be accomplished using the conventional Noyori catalyst. The reduction of esters to alcohols is typically accomplished using metal hydrides. Hydrogenation of carboxylic acids, carbonic acids and their respective derivatives are done using this reagent.[23] Lithium aluminum hydride ($LiAlH_4$), generally abbreviated to LAH, is a powerful reducing agent used in organic chemistry. It is stronger than other reducing agents such as sodium borohydride

due to the weaker lithium-hydrogen bond compared to the boron-hydrogen bond. It is

capable of converting ketones, esters, and carboxylic acids to alcohols; as well as nitro

compounds into amines. Although this method is effective and a widely used method; it

produces large stoichiometric waste and has often complicated workup procedures that

can be mostly time consuming. Moreover, this reaction leads to the production of

dangerous metal oxides and metal hydrides that can affect the environment and

damage especially aquatic life.[24]

$$\text{R}-\overset{\displaystyle O}{\underset{\displaystyle O}{\parallel}}-\text{R'} \quad \xrightarrow[\text{2. } H_2O]{\text{1.(2moles) } LiAlH_4, \text{ diethyl ether}} \quad \text{R}\diagup\text{OH} \ + \ \text{R'}-\text{OH}$$

$$+2AlH_3 + 2LiOH$$
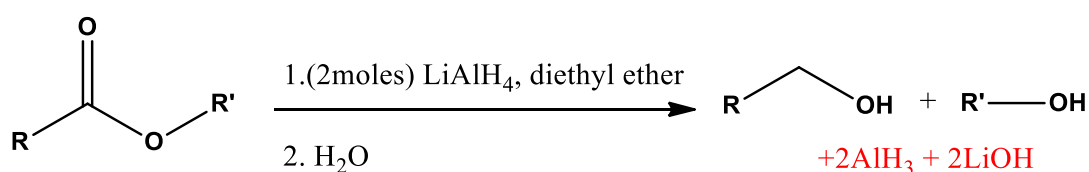
Figure I-3 Ester Hydrogenation using Lithium Aluminum Hydride

3. *Homogenous Hydrogenation Using Transition Metal Complexes*

Using hydrogen gas for ester reduction clearly affords finding a substitute route

for reduction. This route will be environmental friendly and would not produce any

hazardous waste.[25]

The state-of-the-art homogeneous catalysts typically operate at considerably

lower temperatures than their heterogeneous complements, thus having a selectivity

towards alcohol product and is not affected by any other functional groups such as

double bonds.[26] Homogenous transition metal complexes have been used for

hydrogenation of carbonyls and esters in specific. These reactions are proposed to

hydrogenate using the bifunctional mechanism where the ligands are not innocent and

involved in the reaction along with the metal center.[27]

6

Milstein's group succeeded in designing a transition metal complex bearing non-innocent pincer ligand. Milstein reported a bifunctional mechanism encompassing the role of the ligand where aromatization-dearomatization of the PNP or PNN pincer takes place.

C. Bond Activation by Metal-Ligand Cooperation

A unique class of pincer ligands such as [bis(2-di-i-propylphosphinoethyl) amine] coordinate with the metal via three sites: two phosphine arms, and an amine group. These ligands are electron-rich groups and therefore are classified as electron donating groups so they would have the ability to stabilize the unsaturated metal center.
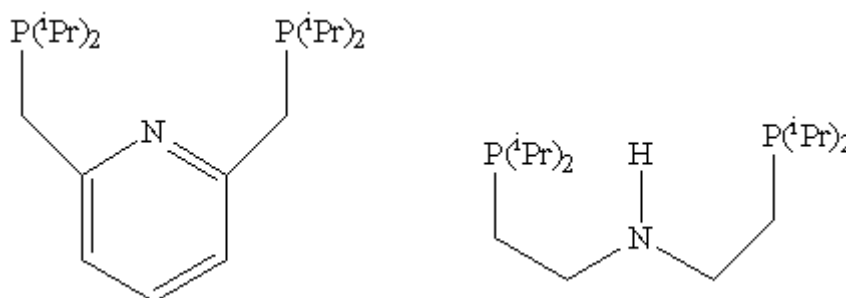
Figure I-4 An Examples of a PNP Pincer ligands in 2-D
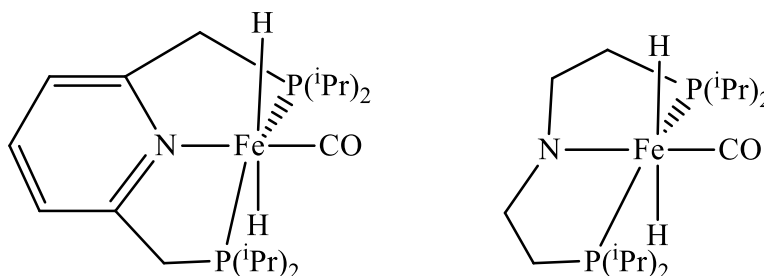
Figure I-5 Milstein's Iron PNP pincer catalyst (left) and Beller's Iron PNP catalyst (right)

Fe(PNP)(CO)(H) is a penta-coordinated iron hydride. Such complexes are known to add H_2 reversibly, with a heterolytic addition to the nitrogen-iron bond to form octahedral trans hydride iron complexes (Figure I.7). [28]
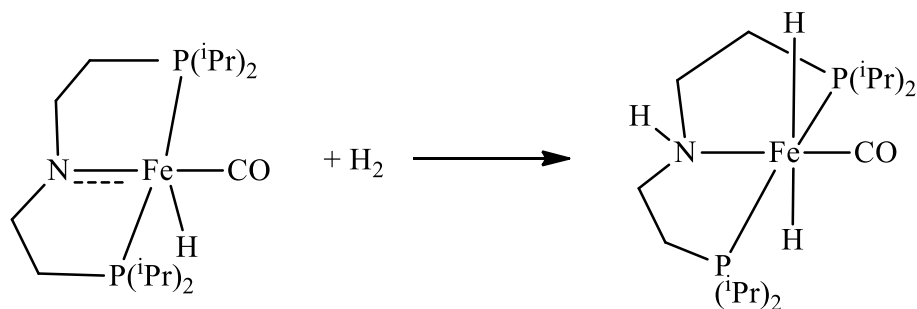
Figure I-6 H_2 addition to iron PNP catalyst via bifunctional mechanism

D. Catalysis by PNP Complexes

Milstein's group reported that the square pyramidal iron complex in presence of H_2 gas catalyzes the hydrogenation of esters into alcohols according to the following equation:
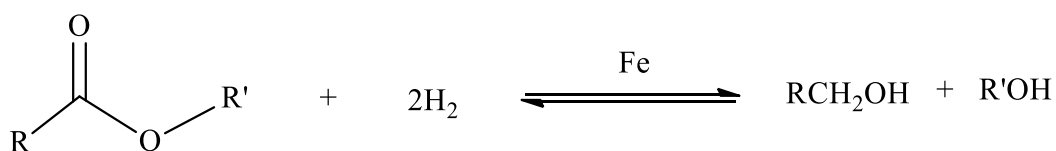
Figure I-7 Hydrogenation of esters into alcohols, catalyzed by iron under H_2 atmosphere

The catalytic hydrogenation of a family of esters to alcohols without the use of precious or toxic metals as catalysts is fortunate. Thus, the iron pincer complex [(^{t}BuPNP)Fe(H)$_2$(CO)] is an efficient catalyst for the selective hydrogenation of trifluoroacetic esters to the corresponding alcohols.

Milstein demonstrated the catalytic hydrogenation of a family of esters to alcohols using iron pincer complex, which showed to be an efficient catalyst for the selective hydrogenation of trifluoroacetic esters to the corresponding alcohols. [29]

As well as this type of metal pincer complexes was further investigated by different groups. For example, Beller and his group succeeded in proposing the first base-free iron-pincer catalyst system for the hydrogenation of various carboxylic acid esters and lactones. [30] Also, Guan had reported a study for the hydrogenation of esters in the presence of the iron pincer complex that has an appreciable efficiency and can be used for industrial processes. They tested it on industrial samples such as methyl laurate, which is found in coconut oil and showed to be applicable under neat conditions. [31]

E. Mechanistic Studies for The Reduction of Esters into Alcohols.

All of the current homogenous catalysts are still not optimal for industrial usage. These catalysts need to be optimized, where optimization involves a detailed knowledge of the mechanism. Several studies have been done and several catalysts have been designed yet none of them has a definite mechanism. A review done by Ikariya, showed numerous catalysts, yet none of them can be promoted to do catalytic reactions for industrial treatments[32]. As a result, investigations for the mechanism for these catalysts is vital and has been done by several groups where most of them were based on the involvement of the ligand in the mechanism, under the name of bifunctional, or metal ligand cooperation (MLC).

1. Bifunctional Mechanism

Metal–ligand cooperation (MLC) or the bifunctional mechanism has become an important concept in catalysis by transition metal complexes. MLC implies that both the metal and the ligand are directly involved in bond activation processes, by contrast to "classical" transition metal catalysis where the ligand (e.g. phosphine) acts as a spectator, while all key transformations occur at the metal center. [33]
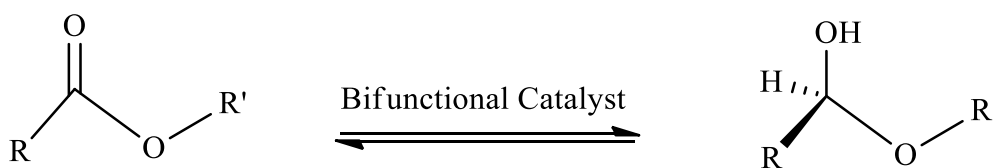
Figure I-8 This equation shows the formation of the hemiacetals by the reaction of esters with any bifunctional catalyst

Several examples of cooperative ligands are listed here. Hydrogenation of ketones and ketimines was investigated by Morris. He designed iron-based catalyst for this type of hydrogenations. [34] Similar natures of iron PNNP ligands, gave an evidence to be very active in the presence of a base to activate the catalyst (Figure I.10). having an alcohol in the system was important for providing hydrogen for the catalytic process or as a solvent. Using hydrogen gas was also an option, however its efficiency was much lower than using the alcohol. [34] The iron pre-catalysts (2) and (3) (figureI-10) [35, 36] was 200 times more efficient than the iron pre-catalysts (1) in turnover frequencies. [37-39] The catalytic activity was affected by the bulkiness of the substituents on the PNNP ligands at the phosphorus position [40] and at the diamine backbone . [37] For the phosphorus position, varying the substituents from Ph to Et to ^{i}Pr to Cy, the activity of the complexes decreased from Ph to Et, and no activity was observed for the complexes with ^{i}Pr or Cy groups on the phosphorus. On the other hand,

the steric effects on the diamine backbone revealed that as the substituents become

bulkier, the activity increases remarkably.
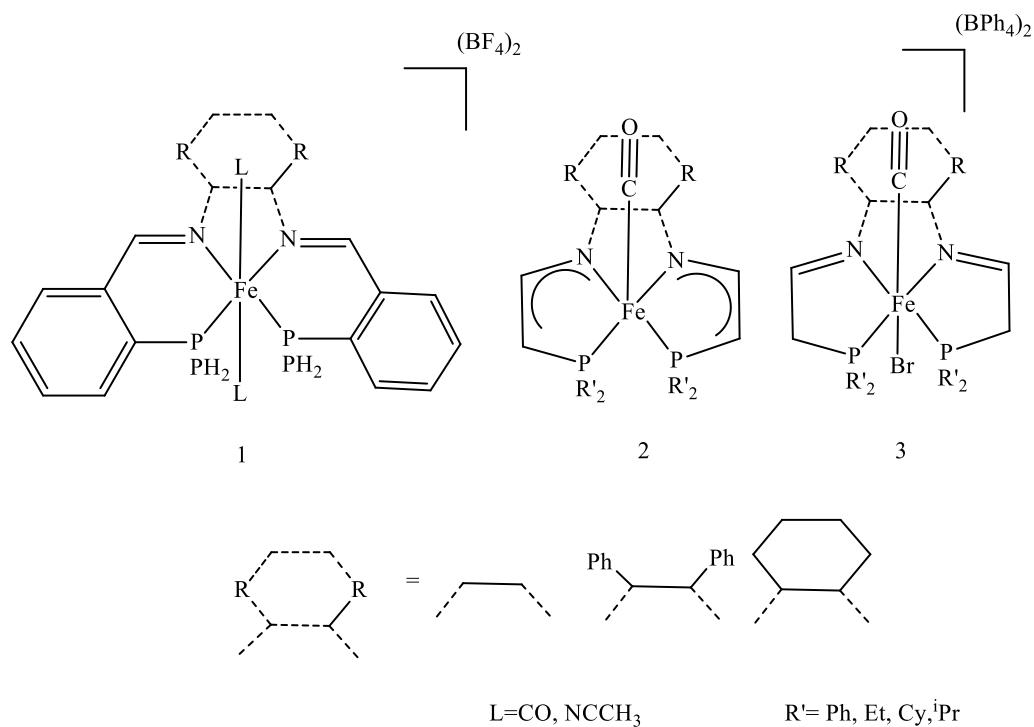
Figure I-9 Three different types of iron pre-catalysts bearing tetradentate ligands (PNNP)

To understand the mechanism for how the catalyst is working, several

experimental and computational studies were conducted. [38, 41-43] As shown in

Figure I.11, The activation of the catalyst was done by the asistance of the base where

the ligand undergoes reduction. Dehydrogenation of the alcohol by the activated

catalyst yielded the carboyl compound and the hydrogenated complex 6. And this

complex works also in the reverse direction for the hydrogenation of carboyls in a

bifunctional outer-sphere mechanism.
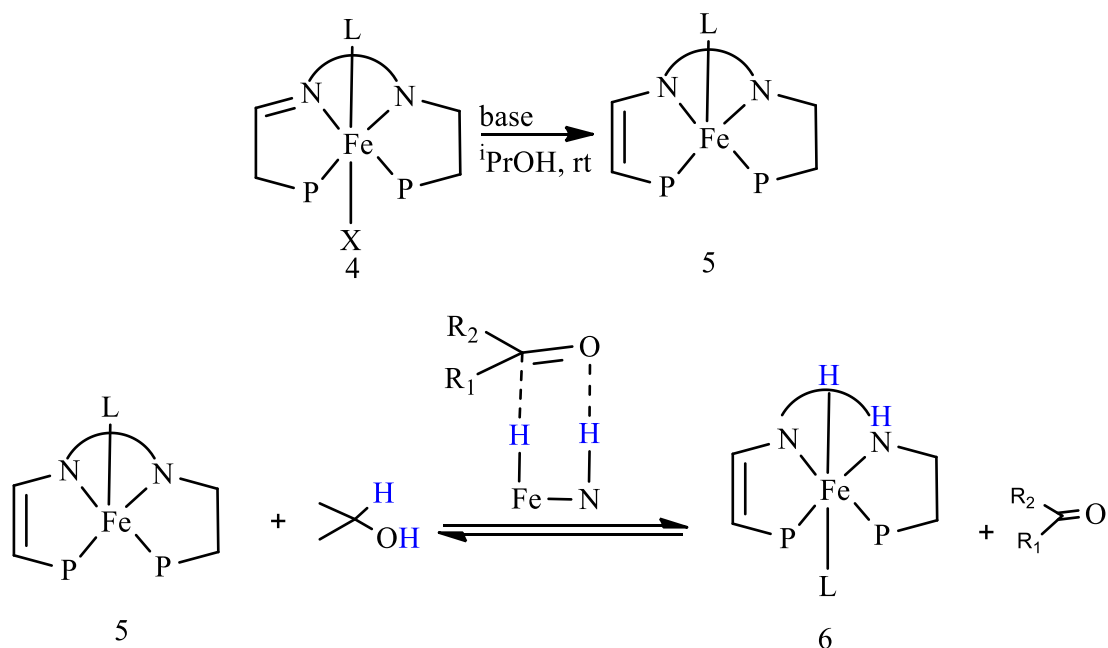
Figure I-10 Proposed catalytic cycle involving pre-catalyst 1

Another mechanism named the metal-ligand cooperation involves dearomatization-aromatization of the pyridine caused by deprotonation-protonation of the benzylic arm of the ligands. [44-46] These ligands were thought to exhibit a non-innocent behavior, and different types of such ligands were synthetized and used in homogenous catalysis. [47, 48] In specific, the chemistry of designing iron type catalyst was studied excessively by several groups, Milstein, [49] Chirik, [50] and Goldman, [51]. Until now, these catalysts are assumed to work in a bifunctional way. For example, Milstein examined the behavior of the iron-PNP pincer catalyst for the hydrogenation of carbonyls including ester, CO_2, aldehydes and ketones. [29, 52-55]
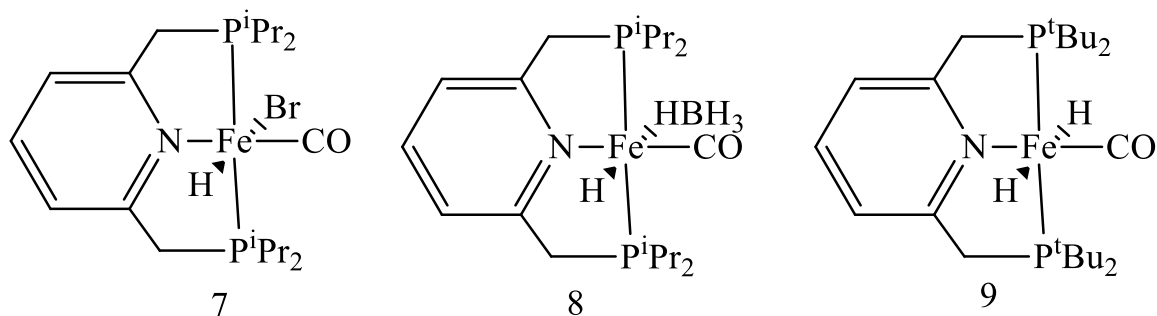
Figure I-11 PNP-Fe pre-catalysts 24-26 used in hydrogenation of CO2, ketones, esters and aldehydes

The complex $FeBr(H)(CO)(PNP\text{-}^iPr_2)$ (7) (Figure I.12) showed to hydrogenate ketones catalytically by the assist of a base and under relatively mild conditions. [53] Exploring its activity and optimizing it, yielded to a conclusion where the presence of ethanol as a solvent, had improved the activity of the catalyst with a 94% yield. On the other hand, a noticeable enhancement was shown by using complex (8) $Fe(BH_4)(H)(PNP\text{-}^iPr_2)$ instead of (7). [54]

As for complex (9) $[Fe(H)_2(CO)(PNP\text{-}^tBu_2)]$, it was a breakthrough for being the first iron complex that is reported for ester hydrogenation.[29] This catalyst was used for the hydrogenation of trifluoro acetic esters into alcohols. This advancement was done under relatively mild temperature (40 °C) and at atmospheric pressure of H_2 that ranges between 5-25 along with producing a quantifiable yield. These types of Fe-PNP pincer complexes were also active for aldehyde hydrogenation. [55]

Gaining mechanistic understandings for the catalytic hydrogenation cycle was done by both experimental and theoretical investigations. Computational and NMR spectroscopic analysis supported that intermediacy of dearomatized/aromatized species. [29, 52-54] All of the theoretical investigations for the mechanism of Fe-PNP pincer

13

complexes agree on the bifunctional taste. A general scheme for the mechanism of carbonyl hydrogenation is shown in figure I.13. This mechanism is summarized by a hydride transfer from the metal to the carbonyl carbon followed by coordination of the terminal oxygen to the metal center (11). The addition of base induces a bifunctional elimination of the alcohol yielding a five coordinated dearomatized pincer complex (12). Regeneration of the catalyst (10) and restoring aromaticity is done by adding the H_2 via metal-ligand cooperation.
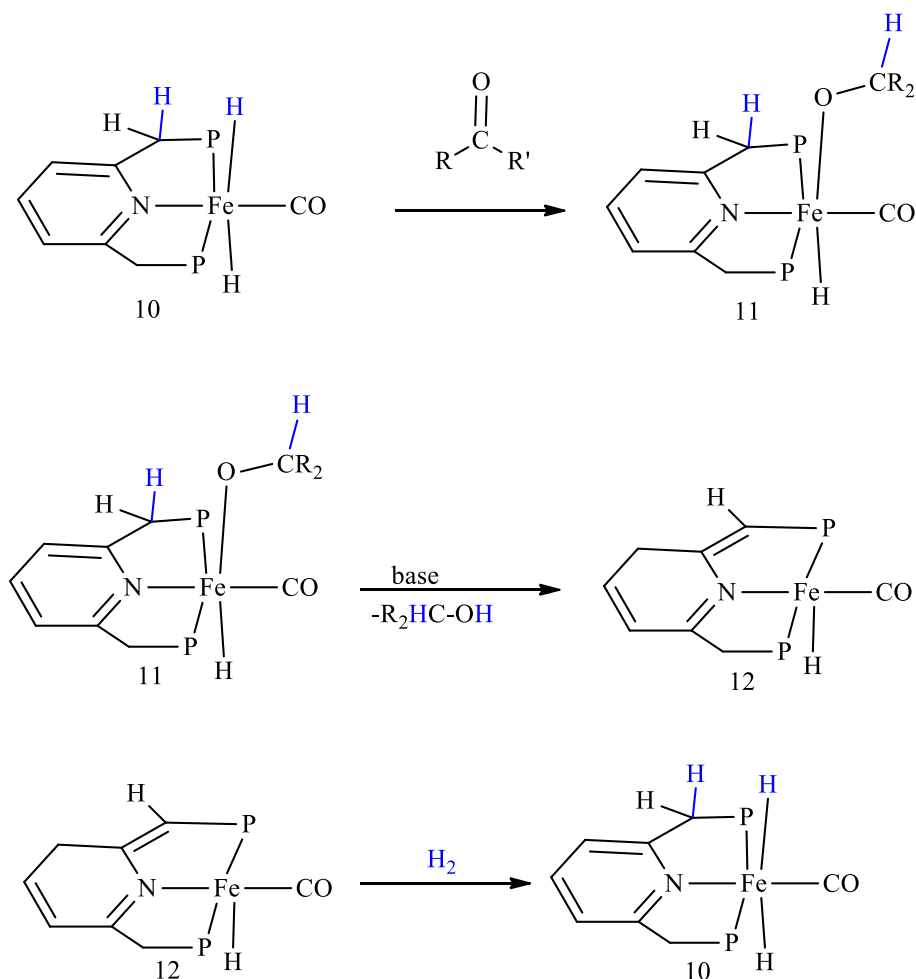
Figure I-12 Proposed mechanism for hydrogenation reactions ($R_2C=O$: ketones, aldehydes or esters)

2. Direct Route Metathesis Mechanism

A new mechanism has been proposed by Hasanayn named as a direct metathesis. [56] He investigated the mechanism for Milstein's catalyst trans-[Ru(H)(OMe)(PNN)(CO)] which was believed to perform in an outer sphere bifunctional Noyori type mechanism, where the pincer ligand plays an important role. Both mechanisms begin with a hydride transfer, where an elongation for the metal-hydride bond followed by a transfer of the hydride to the carbonyl. Hasanayn considered a methylated phosphine arms and according to his DFT calculations, there is a formation of an ion-pair complex between a square-pyramidal cation and a hemiacetaloxide anion in which the formed C−H bond is pointed toward the metal. Rearrangement of the hemiacetaloxide is plausible since there is no covalent bonding between the two ions, so an easy rearrangement can take place where the methoxy oxygen is brought closer to the metal center giving a new minimum on the potential energy surface. The two IP minima are connected by a slippage transition state (3-TS-slip) with a relative free energy of 19.5 kcal/mol, above the separated reactants, which is still plausible to happen.

The overall transformation in Figure I.14 is an unusual organometallic metathesis in which an alkoxide and a hydride are exchanged between the ruthenium metal center and an acyl group. This process is achieved by the ability of the metal to switch the activation of the C−H and C−OR bonds of the hemiacetal oxide by respective coordination of the H and OR groups.
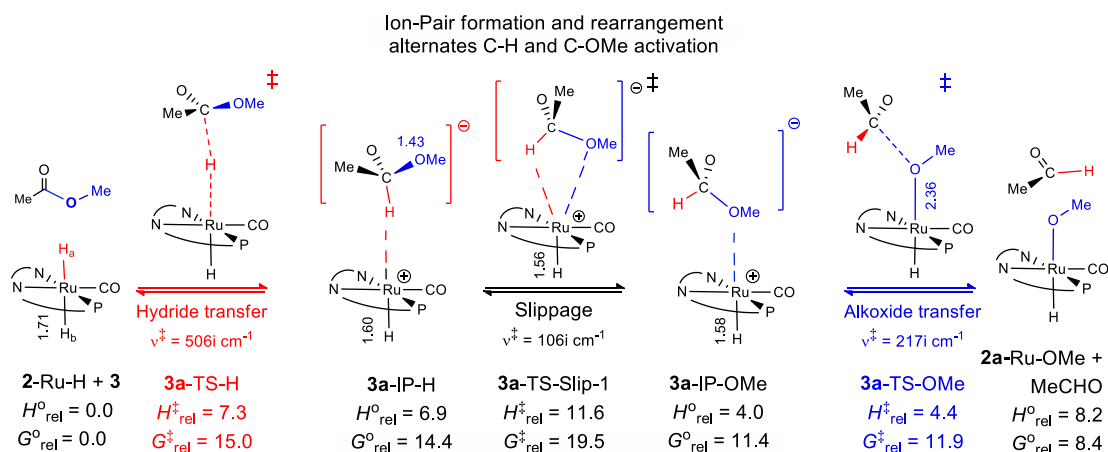
Figure I-13 Calculated H^o_{rel} and G^o_{rel} values of TSs and minima on the PES in the reaction between 2-Ru-H and 3. M06 results are given in kcal/mol at 298 K and 1 atm using a PCM representing THF as solvent. Bond distances are given in Å

Another possibility proposed by Hasanayn would be the coordination of the terminal oxygen of the hemiacetaloxide to give the octahedral hemiacetaloxide Ruthenium complex (2-Ru-HemAc) shown in figure I.15, which is calculated to have a slightly exothermic step. This step can be called a carbonyl group insertion and the reverse is a β-hydride elimination, which is followed by β-OR elimination, so figure I.15 outlines a new insertion and de-insertion reactions involving the alkoxide group. These alkoxide complexes have been observed experimentally; according to Bergens the reaction between a ketone and trans dihydride ruthenium catalyst yielded Ru alkoxides at low temperatures (negative 80 °C) as we can see in figure I.16. [57]
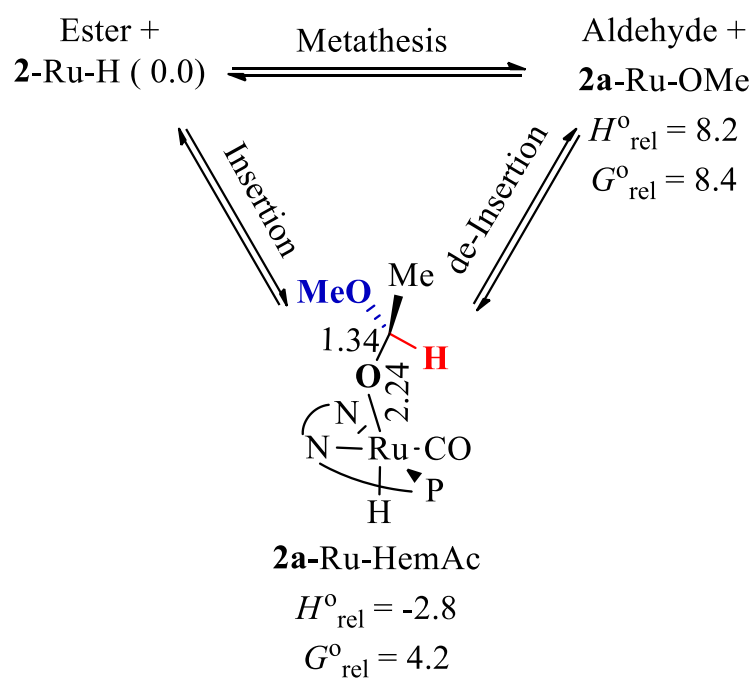
Figure I-14 Three reactions that can be mediated by ion-pair formation and rearrangement. Energies are given in kcal/mol.
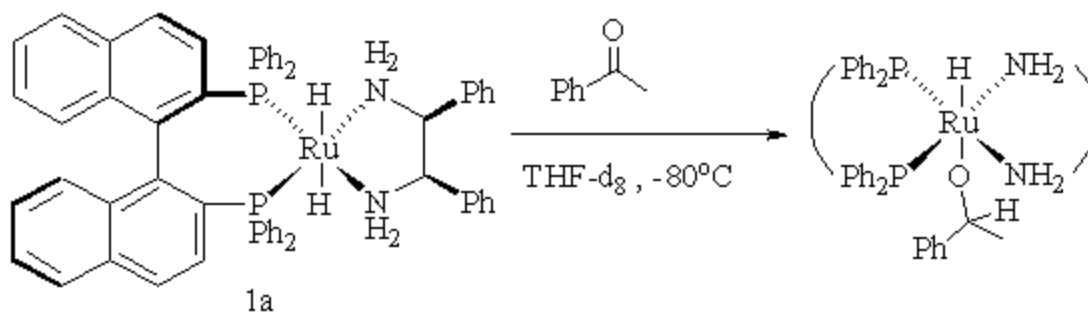
Figure I-15 The reaction between the trans dihydride ruthenium complex and ketone at the mentioned conditions.

CHAPTER II

SYSTEMATIC DFT COMPARISONS OF BIFUNCTIONAL AND ION-PAIR SLIPPAGE MECHANISMS FOR C-OR BOND CLEAVAGE IN HYDROGENATION OF METHYL BENZOATE BY AN OCTAHEDRAL IRON AMINO HYDRIDE CATALYST

A. Introduction

The octahedral iron amino hydride **1**-Fe-H complex (eq 1; $P = P^iPr_2$) is implicated as an active species in the catalytic hydrogenation of esters into alcohols using H_2 and a number of catalyst precursors.[30, 31, 58]
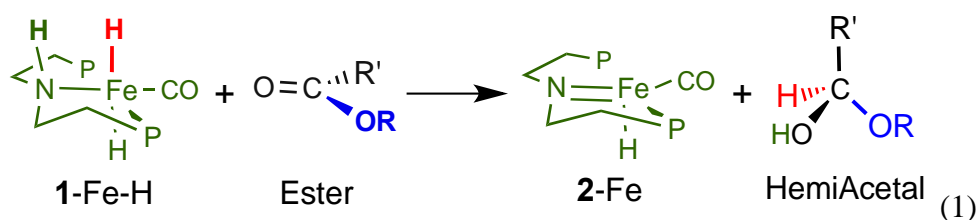
Figure II-1 The reaction between 1-Fe-H and ester to produce hemiacetal

The mechanism in the given system had been postulated to start with a Noyori type bifunctional (or metal-ligand cooperation, MLC) reaction. A hydride from the metal and a proton from the amino group of the ligand are transferred in an outer sphere mode from **1**-Fe-H to the carbonyl group of the ester to produce a hemiacetal and the unsaturated amido complex **2**-Fe (eq 1). Note that **2**-Fe is a known complex that adds H_2 heterolytically to produce **1**-Fe-H.[28]

Complete hydrogenation of an ester yields two alcohol molecules thus requiring hydrogenolysis (or cleavage) of the C-OR bond at some point of the reaction.

A hemiacetal produced in a bifunctional mechanism can in principle fragment into an

alcohol and an aldehyde without the need of a metal catalyst (eq 2). [59] The ester

hydrogenation catalyst would then transform the aldehyde into the second alcohol

(eq 2).

$$\text{Hemiacetal} \rightleftharpoons \text{R'CHO} + \text{ROH} \xrightarrow[\text{[M]}]{+ H_2} \text{R'CH}_2\text{OH} + \text{ROH} \tag{2}$$
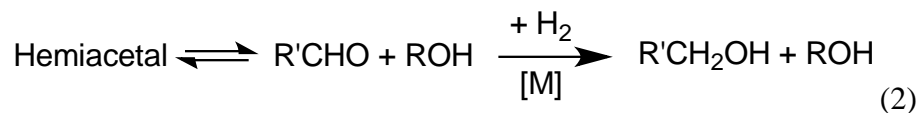
Figure II-2 Fragmentation of the Hemiacetal

The mechanism of ester hydrogenation by **1**-Fe-H has been the subject of two

independent theoretical investigations by Schneider and Wang. [60] The two studies

agree on an initial bifunctional hemiacetal formation stage. They also agree that auto or

solvent assisted hemiacetal fragmentation should be less favored than a fragmentation

catalyzed by the amido intermediate **2**-Fe. However, as described in Scheme 1, the two

studies present opposite scenarios on how the metal mediates the fragmentation.
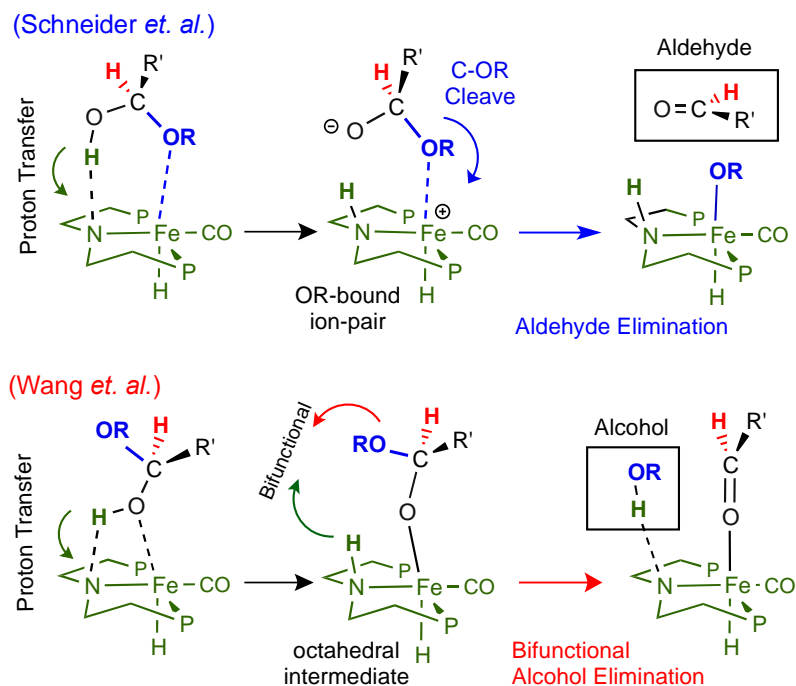
Figure II-3 Two pathways for bifunctional hemiacetal fragmentation by 2-Fe

In Schneider's study the hemiacetal transfers its alcoholic proton and OR group to **2**-Fe to produce an aldehyde and an octahedral metal-alkoxide. To our knowledge this bifunctional mode was first proposed by Wang and coworkers in a study on Milstein's catalyst. [61] However, in their study of **1**-Fe-H, Wang and coworkers propose initial heterolytic addition of the alcoholic OH bond of the hemiacetal to the Fe=N bond of **2**-Fe to give an octahedral hemiacetaloxide intermediate (Scheme 2), followed by a distinct bifunctional transformation that cleaves the C-OR bond to give a metal coordinated aldehyde and an alcohol that is hydrogen bonded to the deprotonated amine.

Previous work at AUB used DFT to study the outer sphere potential energy surface (PES) in the reaction between esters and the dimethyl amino analog of Milstein's octahedral PNN ruthenium hydride catalyst. [56, 62]
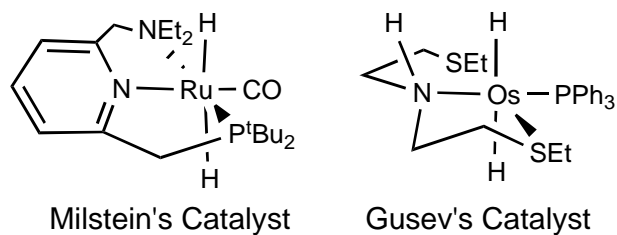
Figure II-4 Milstein's and Gusev's Catalysts

The calculations gave evidence for the accessibility of a direct H/OR metathesis pathway that exchanges a hydride and an alkoxide between a metal center and an acyl group via formation and "slippage" of a hemiacetaloxide ion-pair as shown in Figure II.5.
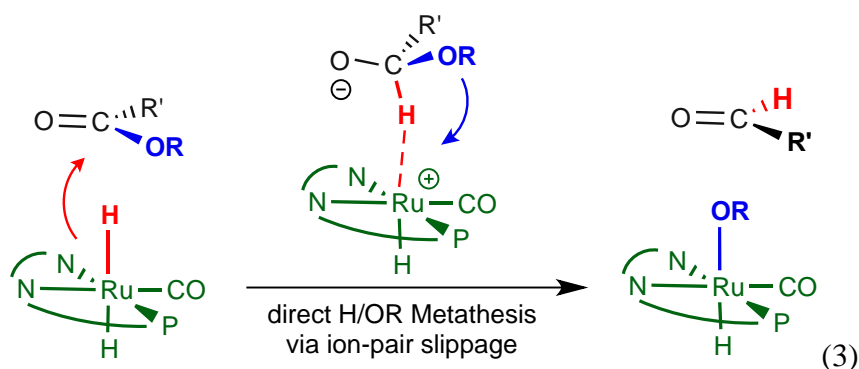
Figure II-5 Direct H/OR metathesis for ester hydrogenation by Ru PNN pincer Complex

This pathway cleaves the C-OR bond without the intermediacy of a hemiacetal, yet it was computed to be at least competitive with the MLC mechanism that is generally accepted in Milstein's chemistry.[45, 63] Similar results were computed for hydrogenation of dimethyl carbonate and methyl formate.[64] More recent calculations by Yang and coworkers on Gusev's amino-hydride ester hydrogenation catalyst

predicted the given H/OR slippage route to be much lower than the bifunctional carbonyl hydrogenation route producing a hemiacetal and osmium amide. [65]

Obviously, ligand deprotonation and ion-pair slippage offer fundamentally different views of a key step in catalysis. Even when a hemiacetal is invoked, the previous propositions on the subsequent C-OR bond cleavage in Figure II.3 correspond to opposite modes with potentially different implications to catalyst design. However, the different studies by Schneider and Wang were done at different levels of theory and they used different alkyl groups on the phosphines of the PNP ligand so the energies of the two fragmentation modes cannot be compared. Furthermore, the study by Schneider reported bifunctional hydrogenation of the carbonyl group of the ester takes place concertedly, whereas Wang reported a stepwise hydride/proton transfer route for the same reaction. **1**-Fe-H and related complexes have emerged as promising low cost versatile catalysts for hydrogenation and acceptorless dehydrogenative coupling of carbonyl compounds [66] as well as in the hydrogenation of nitriles [67] and, most recently, olefins. [68] Thus understanding the nature of the C-OR bond cleavage step in ester hydrogenation can be fundamental to the given chemistry in general. To this end we report here a more complete and systematic DFT investigation of the three route for C-OR bond cleavage in the reaction between **1**-Fe-H and methyl benzoate (**3**). When a solvent continuum representing THF is employed in the calculations the barrier for ligand deprotonation is computed to be smaller than the slippage barrier. However, the highest energy point on the bifunctional PES is computed to be the separated hemiacetal and **2**-Fe and not the proton transfer TS so the slippage and bifunctional pathways come to be competitive. In methanol on the other hand slippage is largely stabilized over

22

ligand deprotonation. Our calculations of hemiacetal fragmentation by **2**-Fe indicate the pathway leading to **2**-Fe-OMe and a free aldehyde should be more probable than the one leading to a metal coordinated aldehyde. Given the very different nature of the PESs investigated, conventional electronic structure methods like the ones employed in the present and previous studies may not be reliable enough to rule out one pathway or another. However, direct ion-pair rearrangement provides the least action path to a nearly thermoneutral H/OR metathesis, and from DFT as well as qualitative perspectives there are no obvious advantages for achieving the same reaction by formation and re-reaction of the separated highly endoergic hemiacetal and amido intermediates.

B.   Computational Methods

The calculations were carried out using Gaussian 09 [69]. Geometry optimization was carried out at the M06L/6-31++(d,p) level [70] in an SMD polarizable continuum using either THF or Methanol as solvent. [71]. Final electronic energies were obtained via single point calculations on the optimized geometries in the respective solvents at the M06L, M06 and ωB97X-D [72] levels using the def2-QZVPP, def2-TZVPP and def2-TZVP basis sets on Fe, hydrogen and the main group elements, respectively. [73] The given three density functionals are widely used in computational organometallic chemistry and had been validated in a number of studies. [74, 75] In particular, Gusev and coworkers demonstrated the M06L level can reproduce the enthalpy of a broad range of organometallic reactions nearly quantitatively. [76]

Similarly, Morris and coworkers used the M06L level to study an iron ketone hydrogenation catalyst and found agreements between computed and measured reaction barriers. [77] The results obtained by the three functionals used in the present work exhibit small variations. For convenience we present and discuss the M06L/THF results, and we compare the effects of using methanol as the solvent continuum and the M06 and ωB97X-D functionals in separate sections.

In electronic structure calculations molecular entropies are obtained using statistical mechanics as a sum of vibrational, translational and rotational terms [78]. When compared with experimental entropies measured in solution, the computed entropies of dissociative/associative reactions can be exaggerated. To illustrate, we consider the simple hemiacetalization of methanol and acetaldehyde. The experimental associative entropy of the reaction is -18 eu. [59] The computed entropy is -40 eu. The discrepancy of each entropy unit at 298 K and 1 atm would translate to a discrepancy of approximately 0.3 kcal/mol in the free energy, so the error can be large and can influence the conclusions when comparing the unimolecular and bimolecular reactions. Wang and coworkers elaborate more on the given problem and they give reference to two simplistic approaches that can mitigate the effect. [60, 61] One approach scales the entropies by 0.5 while the other applies an energy adjustment term of $\pm$ 4.7 kcal/mol to the free energies of bimolecular reactions. Evidently, the two approaches provide major and comparable improvements to the aforementioned entropy of hemiacetalization. In our previous studies on the Milstein system, we scaled the entropies by 0.5, so we do the same in the present work. To make it possible to evaluate the effects of the scaling

factor we report in the figures the scaled entropies and the "raw" def2 electronic energies (E_{M06L}) along with the Gibbs free energies used to make the conclusions.

C. Results and Discussion

1. Conformational and Thermodynamics Considerations

There are three reactions of interest in the present study summarized in Figure II.6 bifunctional hydrogenation (eq 4), H/OR metathesis (eq 5) and carbonyl group insertion (eq 6). Before we address the details of the PES for each reaction, we find it useful to inspect the dependence of their thermodynamics on the conformations of the PNP ligand and the level of theory.
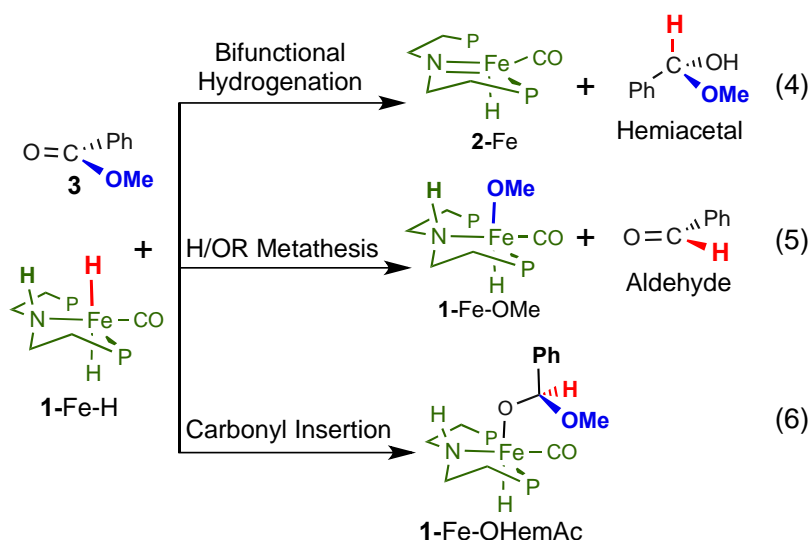
Figure II-6 Three reactions between 1-Fe-H and an ester

Crystallographic studies of complexes relevant to **1**-Fe-H show the aliphatic ^{iPr4}PNP ligand to systematically adopt a symmetrical C_s backbone, so the positions of

25

the isopropyl groups are not differentiated into axial and equatorial. This is different

from the aromatic ^{R4}PNP ligands that have C_2 symmetry. [62, 79]
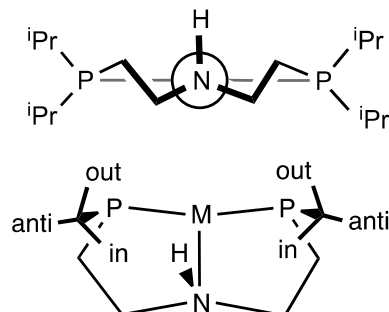
Figure II-7 Clarification figure for representing the iso-propyl group.

However, the conformations of the isopropyl groups in the aliphatic ligand can

still introduce pronounced structural effects on the "cavity" of the catalyst where the

outer sphere reactions take place. In Figure II.8 we consider four such conformations (**a**

– **d**) differentiated by whether the isopropyl C-H bonds are aligned anti to the P-Fe

bond, or pointing inside or outside of a P-N-Fe ring.

1a-Fe-H (E_{rel} = 0.0)   **1b**-Fe-H (E_{rel} = 0.5)   **1c**-Fe-H (E_{rel} = 4.3)   **1d**-Fe-H (E_{rel} = 0.1)

1a-Fe-OMe   **1a**-Fe-OHemAc   **2d**-Fe (five coordinate)
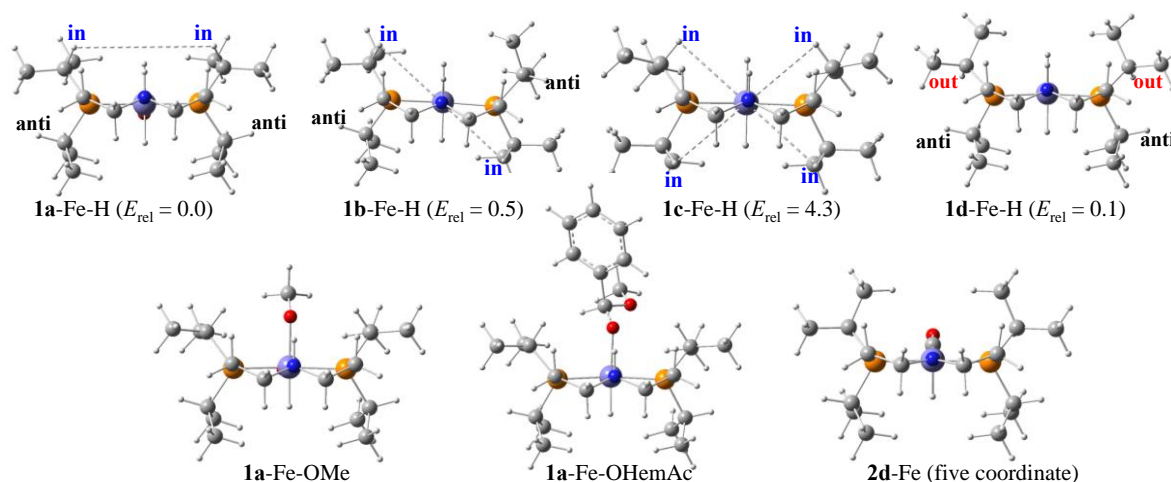
Figure II-8 Four conformations of 1-Fe-H and the lowest energy conformation of
1-Fe-OMe, 1-Fe-OHemAc and 2-Fe (Erel in kcal/mol)

In conformation **a** the C-H bonds of the two isopropyl groups on the same side of the amino-proton are pointing inside the rings whereas the isopropyl C-H bonds on the other side are both anti to the P-Fe bonds thus imparting C_s symmetry to the complex. This conformation is observed in the crystals of a complex in which a borohydride anion bridges two square pyramidal [Fe(^{iPr4}PNP)(CO)(H)] fragments. [80] Conformer **b** has a pseudo-C_2 symmetry with a pair of "diagonal" isopropyl C-H bonds anti to the P-Fe bonds and the other diagonal C-H bonds pointing in the rings. This conformer is observed in a monomoric borohydride derivative of **1**-Fe-H and was considered in the theoretical study by Wang [60] and coworkers. Conformer **c** on the other hand has a pseudo-C_{2v} symmetry with all four isopropyl C-H bonds pointing inside the rings and was used in a recent theoretical study by Jiao and coworkers. [81] Finally, conformer **d** is based on the crystal structure of the unsaturated amido complex **2**-Fe, [28] with a pair of diagonal C-H$_{anti}$ and a pair of C-H$_{out}$ configurations.

For the octahedral *trans*-dihydride **1**-Fe-H, conformers **a**, **b** and **d** are computed to have nearly identical energies, whereas conformer **c** has $E_{rel} = 4.3$ kcal/mol. When a hydride from **1**-Fe-H is replaced by an alkoxide to form **1**-Fe-OMe, conformer **a** is stabilized by 1.7, 2.9 and 3.3 kcal/mol relative to **b**, **c** and **d**, respectively. Conformer **a** is also the lowest energy conformer in the octahedral hemiacetaloxide complex (**1**-Fe-OHemAc), with **b**, **c** and **d** 2.2, 3.1 and 4.9 kcal/mol, respectively, higher in energy. Strikingly, for the unsaturated five coordinate amido complex (**2**-Fe) the crystallographically observed conformer **d** is 5.7, 5.5 or 8.2 kcal/mol more stable than **a**, **b**, and **c**. Presumably conformer **a** creates the biggest

"cavity" over the metal, so it becomes favorable in the octahedral alkoxide and hemiacetaloxide complexes.

Table II.1 Thermodynamic Parameters for Three Reactions Between 1-Fe-H and Methyl Benzoate Defined in Figure II.6. [a]

	Bifunctional Hydrogenation (eq 4)	H/OR Metathesis (eq 5)	Carbonyl Insertion (eq 6)
ΔE_{M06L}	20.7	2.5	-5.3
ΔH_{M06L}	21.3	2.9	-2.4
ΔS (scaled)	8.0	1.8	-21.5
ΔG_{M06L}	18.9	2.4	4.0
ΔG_{M06}	15.0	5.6	3.7
ΔG_{wB97XD}	15.1	4.0	0.0
ΔG_{B3PW91}	12.8	10.7	17.0
$\Delta G_{B3PW91-D3}$	10.4	5.5	-1.5

(a) In THF continuum. G values computed at 298K and 1 atm. Energies are given in kcal/mol, entropies in cal.K^{-1}mol^{-1}.

The thermodynamic parameters for the three reactions in figure II.6 are compared in Table II.1. At the M06L level the bifunctional transformation from the separated **1a**-Fe-H and methyl benzoate (**3**) to the separated hemiacetal and **2d**-Fe (lowest energy conformation) is computed to be highly endothermic ($\Delta H_{M06L} = 21.3$ kcal/mol). At this level of theory, the metathesis is endothermic by 2.9 kcal/mol, and carbonyl insertion is exothermic by -2.4 kcal/mol. For free hemiacetal formation the scaled ΔS is 8.0 eu, which is unexpectedly large since there is no change in the number

of molecules upon this transformation. Even with this favorable term, however, hemiacetal formation comes to be highly endoergic: ΔG_{M06L} = 18.9 kcal/mol (at 298 K and 1 atm). For the metathesis leading to benzaldehyde and **2a**-Fe-OMe ΔS is small (1.8 eu), so ΔH and ΔG are comparable: 2.9 and 2.4 kcal/mol, respectively. Finally, the insertion reaction has an unfavorable entropy of -21.5 eu (after scaling by 0.5), which leads to ΔG_{M06L} = 4.0 kcal/mol, slightly more endoergic than metathesis. The M06 and ωB97X-D results agree with M06L that hemiacetal formation should be approximately 10 kcal/mol less favorable than metathesis, but they predict the carbonyl insertion product to be slightly more favored than metathesis.

Finally, calculations by Jiao and coworkers of eq 4 conducted in part with the B3PW91 functional noted major discrepancies with some M06 results in the study by Wang. Indeed, our B3PW91 calculations predict eq 4, 5 and 6 to be all highly endoergic, ΔG_{B3PW91}= 12.8, 10.5 and 17.0 kcal/mol, respectively. The discrepancy can be attributed to the lack of dispersion interaction terms in the B3PW91 functional. Consistently, when dispersion interactions are added using Grimme's D3 empirical terms [82] as done in the study by Schneider and coworkers for example, the respective B3PW91-D3 energies change into 10.4, 5.1 and -1.5 kcal/mol, in satisfactory agreement with the conclusions obtained by the other three methods in Table II.1.

In brief, the three reactions under consideration have very different character, so it is not surprising for their relative energies to exhibit different dependencies on the level of theory. Nevertheless, the collective results agree that the metathesis and carbonyl insertion reactions leading to octahedral products are thermodynamically much more favorable than the bifunctional transformation into separated **2**-Fe and a

hemiacetal. The results also reveal the energies can be sensitive to the conformations of the isopropyl groups in the PNP ligand. In the following sections we elucidate distinct outer sphere PESs that can lead directly to each of the three products of interest. For all of the stationary points on these PESs conformer **a** is always either comparable or significantly lower in energy than **b** and **d**. As such, we present full results only for the PESs that maintain conformation **a**, and we give only a brief reference to the key results on the other conformations.

D.   PES for Bifunctional Hemiacetal Formation

Figure II.9 considers a PES in which methyl benzoate (**3**) is brought to **1a**-Fe-H such that the carbonyl group is aligned along the HN-FeH bifunctional moiety. The calculations identify a loose complex (**3a**-Plx) between the two molecules characterized by a distance of 2.18 Å between the amino proton of the ligand and the carbonyl oxygen of the ester. The electronic energy of **3a**-Plx relative to the separated reactants is -7.4 kcal/mol. Comparable energies are computed at the M06 (-7.9 kcal/mol) and ωB97X-D (-9.3 kcal/mol) levels. The geometric parameters in **3a**-Plx are not supportive of the presence of a hydrogen bond between the carbonyl oxygen and the amino proton or an interaction between the hydride and the carbonyl carbon. Thus the negative ΔE_{Plx} values appear to follow from dispersion interactions which are accounted for in different weights by the given three density functionals.[83]
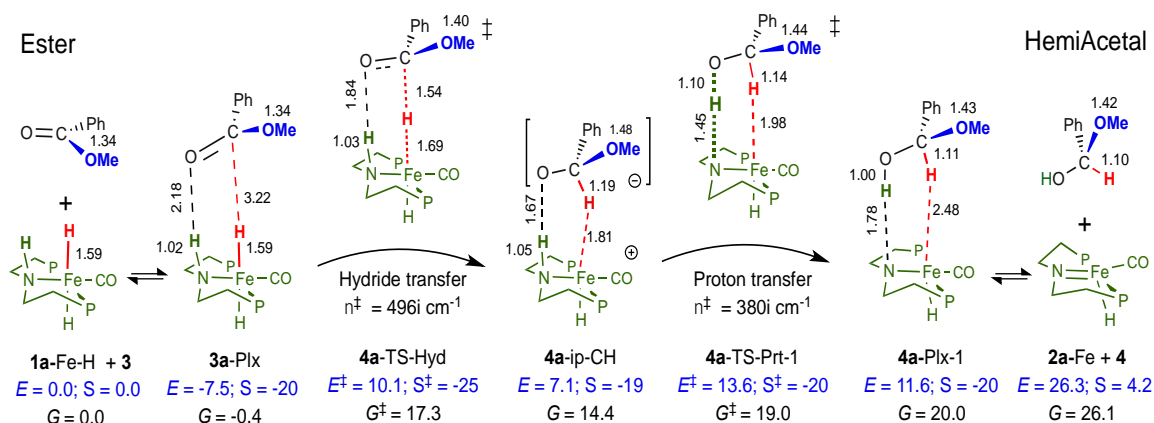
Figure II-9 PES for hemiacetal formation from 1a-Fe-H and 3. M06L//def2/THF results in kcal/mol and Å

After **3a**-Plx there is a transition state (TS) for a localized hydride transfer step from the metal to the carbonyl of the ester (**4a**-TS-Hyd). This leads to an ion-pair in which the newly formed CH bond of the hemiacetaloxide is pointed to the metal at 1.81 Å (**4a**-ip-CH), thus suggesting some degree of anagostic bonding. **4a**-TS-Hyd and **4a**-ip-CH exhibit decreased bond distances between the terminal oxygen of the ester and the amino proton, 1.84 and 1.67 Å, respectively, clearly reflecting an increased degree of hydrogen bonding as the carbonyl group acquires increased negative electric charge. The electronic barrier to hydride transfer relative to **3a**-Plx is substantial ($\Delta E^{\ddagger} = 17.6$ kcal/mol) and the reaction thermodynamics are unfavorable by 14.6 kcal/mol.
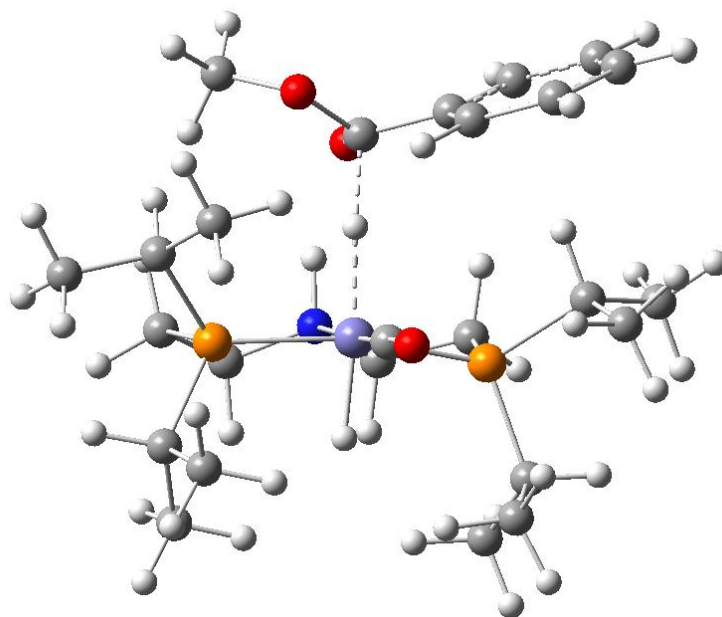
Figure II-10 3D structure for the hydride transition state

Bifunctional hydrogenation requires deprotonation of the amino group of the
PNP ligand by the terminal oxygen of the hemiacetaloxide. The TS for this step (**4a**-TS-
Prt-1) is characterized by large degree of N--H bond cleavage (1.45 Å) and a short H--O
distance (1.10 Å) thus implying a late product-like TS. The step leads at first to a
hemiacetal complex (**4a**-Plx-1) in which the alcoholic proton is hydrogen bonded to the
amide. Proton transfer starting from **4a**-ip-CH encounters an electronic barrier of $\Delta E^{\ddagger} =$
6.5 kcal/mol, which puts **4a**-TS-Prt-1 3.5 kcal/mol above **4a**-TS-Hyd. In spite of the
strong hydrogen bond in **4a**-Plx-1, proton transfer lacks any significant thermodynamic
driving force, $\Delta E = +2.0$ kcal/mol relative to **4a**-ip-CH. Interestingly, the computed
Gibbs free energy of **4a**-Plx-1 is one kcal/mol *above* **4a**-TS-Prt-1.
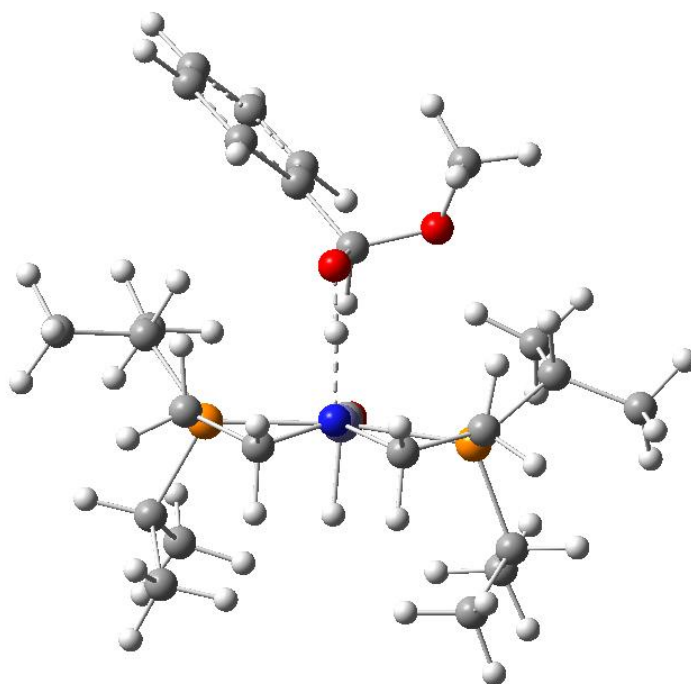
Figure II-11 3D structure for the Proton transition state

To further support that bifunctional hydrogenation takes place stepwise we conducted intrinsic reaction coordinate calculations (IRC) originating from **4a**-TS-Hyd and **4a**-TS-Prt-1 (Figure II.12). The results confirm the assignments, and they show that after hydride transfer is completed, the hemiacetaloxide has to undergo a large degree of displacement from its equilibrium position in **4a**-ip-CH in the direction of the amine before it reaches the proton transfer TS, although there is no significant change in the energy in this segment. The possibility of concerted bifunctional TSs in ketone hydrogenation by Noyori's catalysts was initially supported by gas phase calculations. [14] However, more recent calculations suggest stepwise hydrogenation is more likely to be the norm with amino hydride complexes. [84, 85]
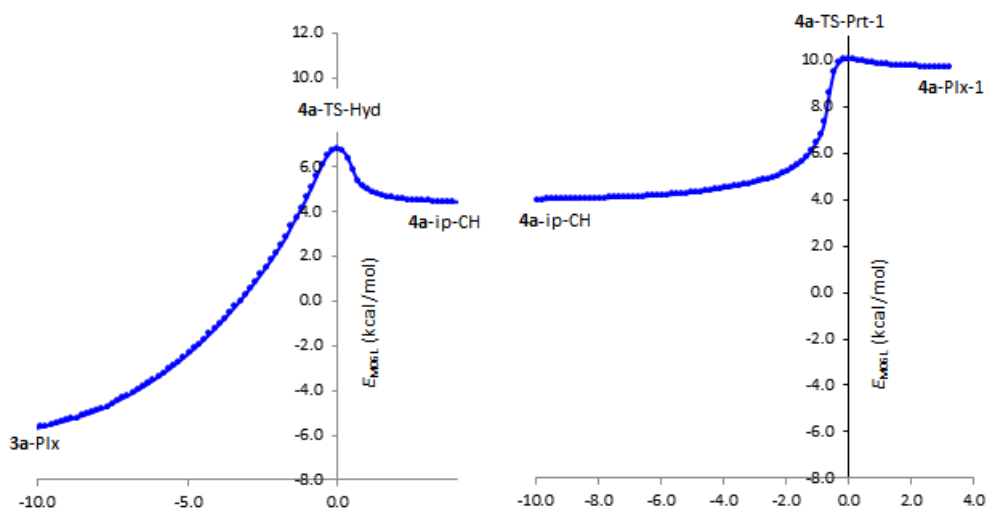
Figure II-12 M06L/6-31++(d,p)/THF IRCs originating from 4a-TS-Hyd and 4a-TS-Prt-1. IRC in Bohr.amu1/2 and E in kcal/mol relative to the separated reactants.

All of the stationary points discussed so far are for conformer **a** defined in Fig.II.8. Accordingly, dissociation of the hemiacetal from **4a**-Plx-1 would yield at first a higher energy conformer of the unsaturated amido complex **2**-Fe. Consistent with the presence of a strong hydrogen bond between the hemiacetal and the amide, the "vertical" dissociation energy of the hemiacetal defined for the transformation from **4a**-Plx-1 to **2a**-Fe is calculated to be large: $\Delta E_{diss} = 14.7$ kcal/mol (or 13.4 and 16.9 kcal/mol at the M06 and ωB97X-D levels, respectively). Evidently, accurate evaluation of a possible role for the bifunctional mechanism in catalysis will rest on the entropy of hemiacetal dissociation from **4a**-Plx, which we know can be problematic to calculate. However, the computed scaled vertical ΔS_{diss} is 24 eu, which seems perfectly reasonable for the step. This value affords $\Delta G_{diss} = 6.1$ kcal/mol, which puts the vertical separated hemiacetal and **2a**-Fe at 26.3 kcal/mol relative to the reactants or 7.1 kcal/mol higher than **4a**-TS-Prt-1.

Figure II.8. shows that conformations **a**, **b** and **d** of **1**-Fe-H have comparable

energies. When hydrogenation is calculated in conformation **b**, all of the stationary

points are raised by 1 - 2 kcal/mol, and the vertical dissociation products continue to

make the highest energy point on the Gibbs free energy profile. On the other hand, the

highest energy point on the PES in conformation **d** which correlates with the lowest

energy conformation of **2**-Fe is 25.0 for **4d**-TS-Hyd, close to the separated vertical

products on path **a** (26.3 kcal/mol).

In summary, our calculations concur with the results reported by Wang that the

bifunctional PES for ester hydrogenation by **1**-Fe-H starts with a localized hydride

transfer step leading to an ion-pair minimum and not concertedly. This is true for all

conformations of **1**-Fe-H, though the barrier varies from 17.3 in **1a**-Fe-H to 25.0

kcal/mol in **1d**-Fe-H ($G^{\ddagger}_{M06L}$; relative to the separated reactants). The energy of **4a**-ip-

CH from the localized hydride transfer step is much lower than either the complexed or

separated hemiacetal product. In the following two sections we start with **4a**-ip-CH and

we investigate two ion-pair slippage modes, one leading to H/OR metathesis and one to

carbonyl group insertion.

E.   PES for Direct H/OR Metathesis

In **4a**-ip-CH the terminal C-O bond of the hemiacetaloxide is nearly eclipsed

with the Fe-N bond of the square pyramidal metal fragment (d1 = 11.5°) and the α-CH

bond is nearly eclipsed with the hydrogen bond between the amino proton and the

terminal oxygen (d2 = -8.8°; Fig. II.14.). In this geometry the phenyl and methoxy

groups on the anion are both oriented upward away from the metal. As we can see in

Figure II.13 below.
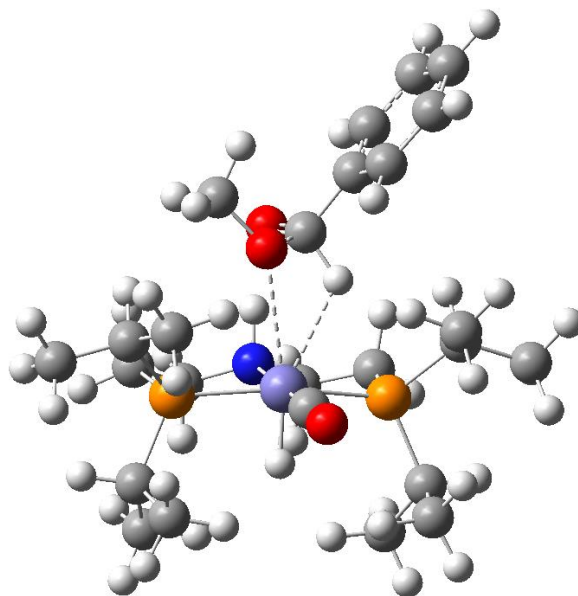
Figure II-13 3D structure for the slippage transition state
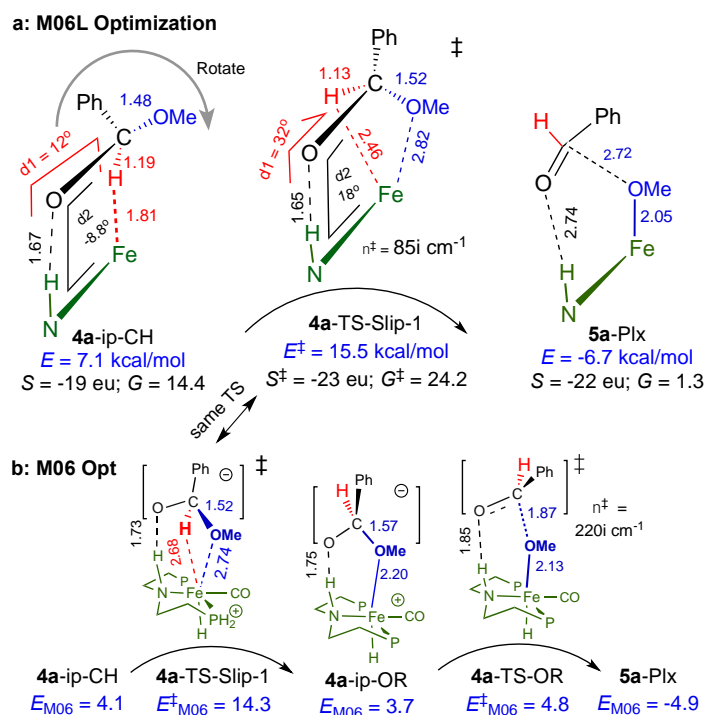
Figure II-14 Ion-Pair slippage completing H/OR metathesis.
Energies in kcal/mol relative to the separated 3 and 2a-Fe-H.

The C-H bond in **4a**-ip-CH is 1.19 Å, implicating activation due to interaction

with the metal. Therefore, hydride back transfer from **4a**-ip-CH to the metal to give **1a**-

Fe-H and an ester has only a small barrier ($\Delta E^{\ddagger} = 3.0$ kcal/mol; Fig. II.9.) The idea of

the proposed direct ion-pair α-H/OR slippage mode is that, by analogy with C-H

activation, coordination of the alkoxy group of the hemiacetaloxide to the metal would

activate the C-OR bond making it kinetically feasible to cleave into the octahedral **1a**-

Fe-OMe and an aldehyde. In other words, we consider an initial hydride transfer from

the metal to the carbonyl of the ester to make a hemiacetaloxide anion followed by an

alkoxide transfer from the hemiaetaloxide to the metal. If we start with **4a**-ip-CH the

least action path to bring the OMe group to the metal would be a trivial rotation, or

"slippage", of the three groups on the α-carbon with respect to the terminal C-O bond.

We identified a TS for this rotation at d1 = 32º and d2 = 18º (**4a**-TS-Slip-1; Fig. II.14.).

Importantly, the given TS retains a strong hydrogen bond between the terminal oxygen

of the anion and the amino proton of the ligand (NH--O = 1.63 Å). As the rotation takes

place in the direction of the TS, the distance between the metal and the α-hydrogen of

the anion increases from 1.8 to 2.5 while the Fe--OMe distance decreases from 3.4 to

2.8 Å. The imaginary frequency in **4a**-TS-Slip-1 is small ($85i$ cm^{-1}) and has coordinates

unambiguously characteristic of a motion that exchanges coordination of the α-H and α

-OMe groups to the metal.

Based on previous results on the Milstein system we anticipated to identify a

minimum after **4a**-TS-Slip-1 for an ion-pair in which the OMe group of the

hemiacetaloxide is coordinated to the metal. However, the search for this minimum at

the M06L/THF level always leads to C-OMe cleavage and converges to an adduct

between benzaldehyde (**5**) and the octahedral **1a**-Fe-OMe (**5a**-Plx in Figure II.14). The

previous studies were done with the M06 functional. Indeed, when the M06 functional

is used in geometry optimization in the present study a minimum for **4a**-ip-OR can be

identified along with distinct TS for a localized C-OMe cleavage step (**4a**-TS-OR)

connecting **4a**-ip-OR to **5a**-Plx. These stationary points are included in Figure II.14. As

expected, the C-OMe bond in **4a**-ip-OR (1.57 Å) is longer than in **4a**-ip-CH (1.48 Å).

Consistently, the M06 electronic barrier from **4a**-ip-OR to **4a**-TS-OR is only 1.1

kcal/mol. This minor barrier for C-OMe cleavage appears to be simply absent on the

M06L PES. Thus, the M06 and M06L results both indicate that once **4a**-TS-Slip-1 is

crossed C-OR bond cleavage would proceed directly to the metal-alkoxide and

aldehyde. We support this conclusion with IRC-M06L calculations in a subsequent

section. Note that upon transformation from **4a**-ip-CH to **4a**-TS-Slip-1 (Fig. II.14) the C-H bond contracts from 1.19 to 1.13 Å whereas the C-OMe bond stretches from 1.46 to 1.52 Å. This means a significant degree of activation is already exerted on the C-OMe bond in **4a**-TS-Slip-1.
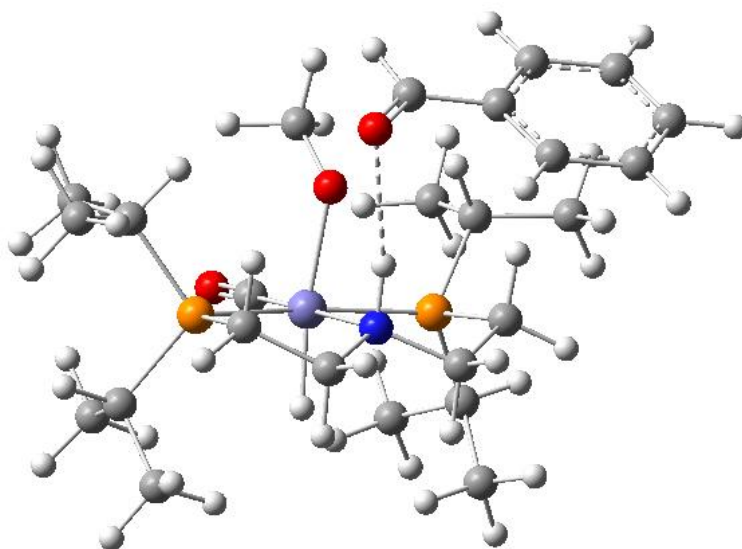
Figure II-15 3D structure for **5a**-Plx

The computed barrier for the transformation from **4a**-ip-CH to **4a**-TS-Slip-1 in THF is 8.4 kcal/mol ($\Delta E^{\ddagger}_{M06L}$, Fig. II.14). The corresponding slippage barriers in the Milstein and Gusev systems were both near 4 kcal/mol. The α-H/OR slippage TS requires that both the C-H and OR groups of the hemiacetaloxide be simultaneously oriented to the metal and exhibit increased degree of ion-pair dissociation compared to the CH-bound ion-pair minimum. We previously argued that the amino arm in the PNN ligand of Milstein's catalyst creates an "opening" over the ruthenium center that allows ion-pair rearrangement to take place without much steric hindrance. Presumably, the same applies to Gusev's SNS ligand where each sulfur donor has only one ethyl substituent, but not in the isopropyl PNP ligand considered in the present study.

Furthermore, because the equilibrium distance between the metal and the CH bond of the hemiacetaloxide in the ion-pair is shorter in the iron compared to the ruthenium and osmium catalysts (approximately 1.8 vs 2.0 Å) the energy input needed to pull the ions apart to reach TS-Slip-1 will be greater in the iron system. We note however that the slippage barrier is computed to be sensitive to the nature of the solvent continuum applied in the calculations. In methanol for instance the slippage $\Delta E^{\ddagger}_{M06L}$ is reduced to only 4.3 kcal/mol.

F.   PES for H/OR Metathesis via Carbonyl Insertion and De-insertion

In Figure II.14, the slippage from **4a**-ip-CH brings the OMe group to the metal to achieve H/OR metathesis. In Figure II.16, we consider a variation on the same slippage mode that orients the terminal anionic oxygen of the hemiacetaloxide to the metal to complete a net carbonyl group insertion into **1a**-Fe-H. The TS for this step (**4a**-TS-Slip-2) has $G^{\ddagger}_{M06L} = 23.8$ kcal/mol, similar to **4a**-TS-Slip-1. The insertion thermodynamics at the M06L level is 4.0 kcal/mol, slightly less favored than H/OR metathesis.
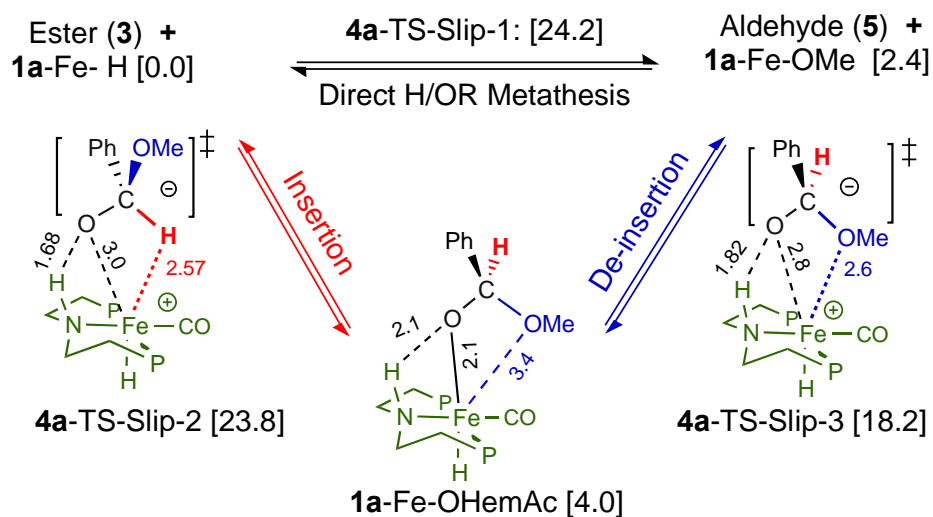
Figure II-16H/OR metathesis via carbonyl group insertion and de-insertion (values in brackets are GM06L/THF energy in kcal/mol).

In the octahedral insertion product, **1a**-Fe-OHemAc the methoxy group is in a close proximity to the metal (3.4 Å). From this point, it is possible to define a third slippage mode that exchanges the coordination of the terminal anionic oxygen with the alkoxy group to eliminate an aldehyde. In the TS for this rearrangement (**4a**-TS-Slip-3) the OMe group is brought to 2.6 Å from the metal center and the terminal oxygen is pulled to 2.8 Å. $G^{\ddagger}_{M06L}$ of **4a**-TS-Slip-3 is 18.2 kcal/mol, significantly lower than **4a**-TS-Slip-2. Thus the sequence of ester insertion and aldehyde de-insertion in Fig. II.16 should be competitive with direct H/OR slippage. In the Milstein system too TS-Slip-3 was much lower than TS-Slip-2.
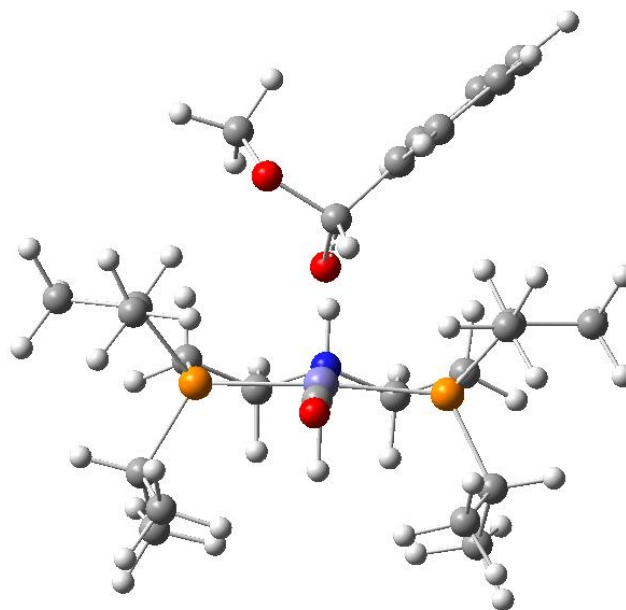
Figure II-17 3D Structure for the **1a**-Fe-OHemAc

G.   Gibbs Free Energy Profiles

The standard state Gibbs free energy profiles of the bifunctional and H/OR metathesis reactions computed with three different functionals and two solvent continuums are compared in Figure II.18 (at 298 K and 1.0 atm). For the bifunctional PES computed at the M06L/THF level, the proton transfer TS is slightly higher in energy than **1a**-TS-Hyd (19.0 vs 17.3 kcal/mol). However, proton transfer does not have any thermodynamic driving force and the highest energy point on the bifunctional PES is for the vertical dissociated hemiacetal and **2a**-Fe products (26.1 kcal/mol). This analysis assumes that the activation entropy for hemiacetal dissociation from **4a**-ip-CH is the same as the thermodynamic ΔS_{diss} (24 eu). A more realistic $\Delta S^{\ddagger}_{diss}$ is more likely to be smaller than ΔS_{diss}, which should further raise the highest energy point on the bifunctional PES.
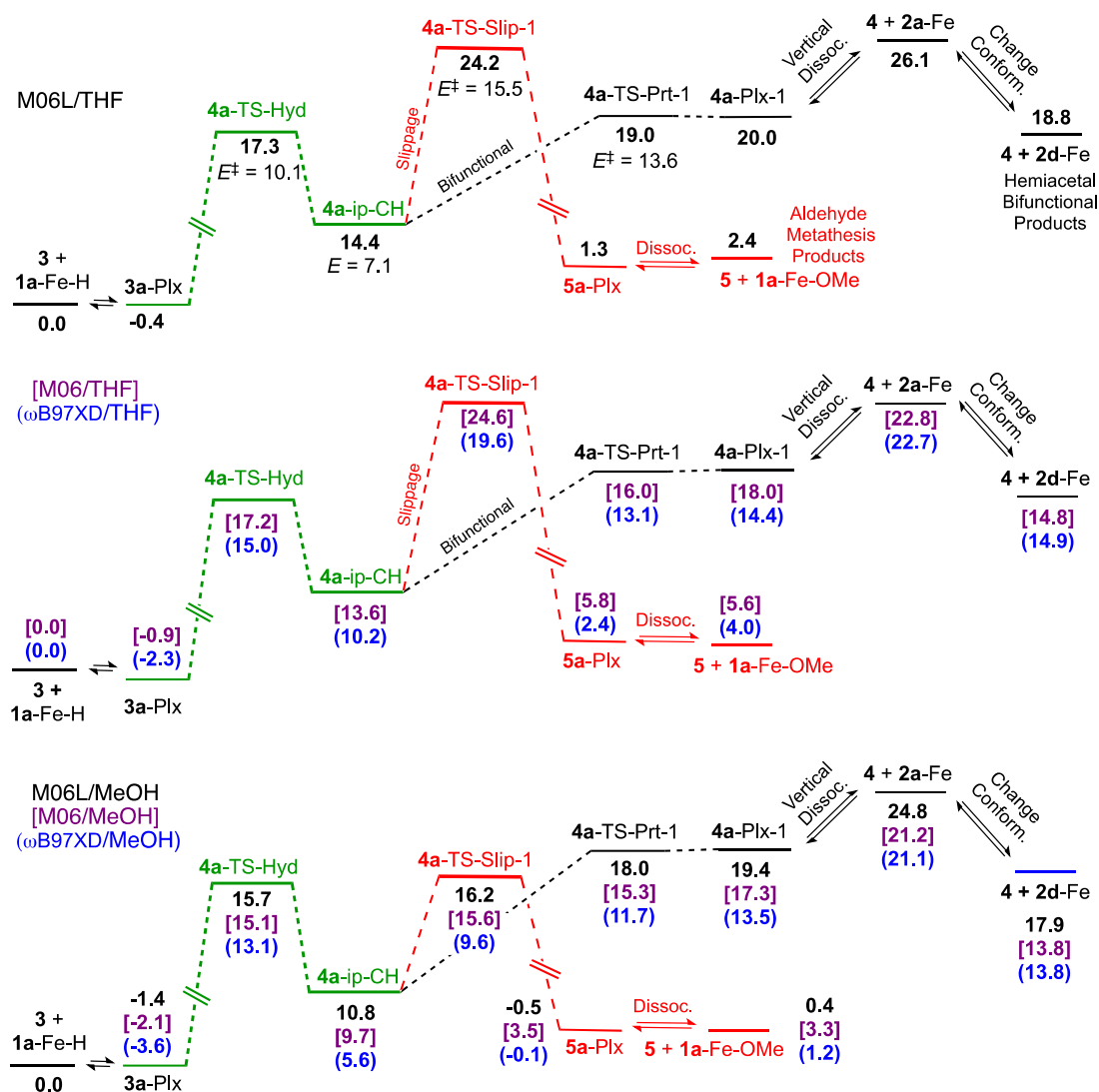
Figure II-18 Gibbs free energy profiles for hemiacetal and aldehyde formation from **1a**-Fe-H and **3** (at 298 K and 1 atm in kcal/mol, using entropies scaled by 0.5).

The highest energy point on the metathesis PES in THF is 24.2 kcal/mol for **4a**-TS-Slip-1. However, unlike proton transfer, the transformation from **4a**-ip-CH into **5a**-Plx mediated by TS-Slip-1 is highly exoergic (ΔG_{M06L} = -13.1 kcal/mol), and the separated aldehyde and **1a**-Fe-OMe have G_{M06L} = 2.4 kcal/mol. This mean that the thermodynamically more favorable H/OR metathesis should be kinetically compatible with bifunctional hydrogenation even though **4a**-TS-Prt-1 is lower than **4a**-TS-Slip-1. A similar conclusion is obtained at the ωB97X-D level (using the M06L geometries and

associated thermal and entropy correction terms). At the M06 level, on the other hand the vertical bifunctional products (22.8 kcal/mol) are slightly stabilized compared to **4a**-TS-Slip-1 (24.6 kcal/mol).

When a polarizable continuum representing methanol as solvent is applied in place of THF in the calculations, $G^{\ddagger}_{M06L}$ and $G^{\ddagger}_{wB97XD}$ of TS-Slip-1 become *lower* by approximately 2.0 kcal/mol than TS-Prt-1, or 8 kcal/mol lower than vertical separated bifunctional (hemiacetal) products. At the M06/MeOH level the slippage and proton transfer TSs become similar. Interestingly, the highest energy point on the ωB97X-D/MeOH metathesis PES is the hydride transfer TS and not slippage: $G^{\ddagger}_{wB97XD} = 13.1$ and 9.6 kcal/mol, respectively. At this level the proton transfer TS (11.7 kcal/mol) is also slightly lower than TS-Hyd, but the vertical dissociated hemiacetal products remain high in energy (21.1 kcal/mol). The reported catalysis experiments were done in THF or toluene. Nevertheless, given the simplistic nature of the solvent continuum methods, the results obtained in methanol should be relevant to enforce the conclusions from the THF calculations that the direct slippage pathway to metathesis should be at least competitive with the bifunctional route. Finally, the given three levels of theory agree **4a**-TS-Slip-1 and **4a**-TS-Slip-2 should have similar energy and to be approximately 5 kcal/mol above **4a**-TS-Slip-3.

H.   Hemiacetal Fragmentation by 2a-Fe

This section addresses the nature and energy of three distinct hemiaetal fragmentation pathways by **2a**-Fe. Reaction between the two species would start in

formation of an adduct in which the alcoholic proton of the hemiacetal (**4**) is hydrogen

bonded to the amido nitrogen of **2a**-Fe. Adduct **4a**-Plx-1 produced on the hydrogenation

PES in Fig. II.9 has the α-CH bond of the hemiacetal pointing to the metal. The three

fragmentation reactions described in Fig. II.19 start with three new adducts, one

coordinated to the metal by the OMe group (**4a**-Plx-2) and two coordinated by the

hydroxyl group (**4a**-Plx-3 and **4a**-Plx-4). From each adduct we identify a barrierless

proton transfer TS ($\Delta E^{\ddagger} \approx +1$, or $\Delta G^{\ddagger} \approx -1$ kcal/mol) that returns the alcoholic proton of

the hemiacetal back to ligand.
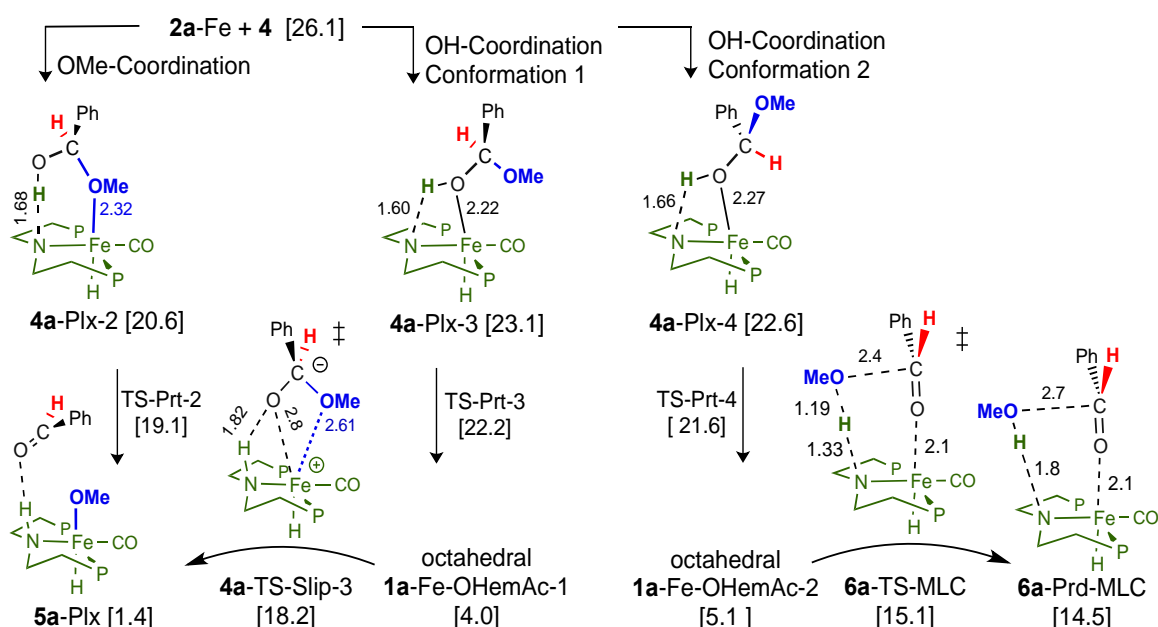
Figure II-19 Hemiacetal fragmentation by 2a-Fe. Values in bracket are the
M06L/def2/THF. Gibbs free energies relative to the separated ester and 1a-Fe-H (in
kcal/mol).

 A localized proton transfer alone in **4a**-Plx-2 would give at first an OMe-bound

hemiacetaloxide ion-pair but, as noted before, no such minimum can be identified on

the M06L PES as the OMe group of the hemiacetaloxide cleaves when it gets close to

the metal. This means that once the hemiacetal reaches the metal in the given

45

conformation it will undergo barrierless fragmentation into an aldehyde an octahedral

alkoxide. These are the same H/OR metathesis products obtained in Fig. II.16 by ion-

pair slippage. This fragmentation mode is investigated further by IRC calculations in

Fig. II.20.
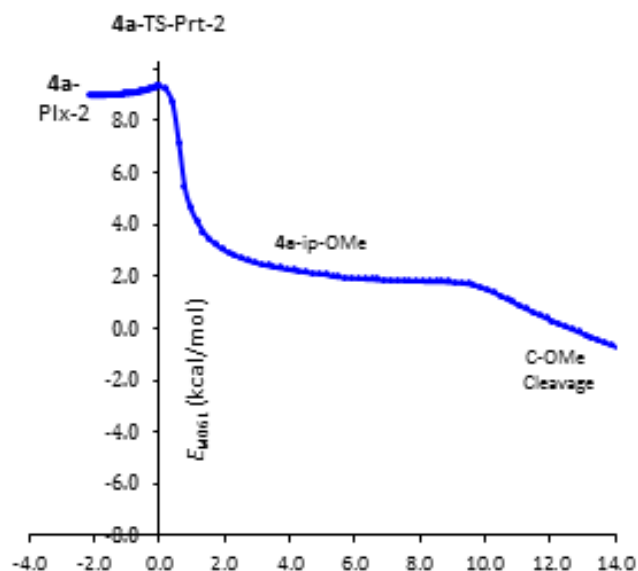
Figure II-20 IRC originating from 4a-TS-Prt-2.IRC in Bohr.amu$^{1/2}$ and E_{M06L} in kcal/mol relative to the separated ester and **1a**-Fe-H.

The IRC$_{M06L}$ highlights the absence of any significant barrier from **4a**-Plx-2 to

4a-TS-Prt-2 ($\Delta E^{\ddagger} \approx$ +1 kcal/mol). The IRC past the TS can be divided into three

segments. First there is a sharp drop in the energy as the proton completes its transfer to

the ligand. In this region the C-OMe bond lengthens by approximately 0.1 Å, from 1.5

to 1.6 Å. Next, there is an energy plateau for minor conformational changes that fit the

hemiacetaloxide in the catalyst cavity. Finally, there is a region of another steep energy

descent due to C-OMe bond cleavage. Thus in spite of the absence of a minimum for an

OMe bound hemiacetaloxide ion-pair on the M06L PES, **4a**-TS-Prt-2 itself is still

consistent with a localized proton transfer TS, as opposed to a concerted bifunctional

TS in which the proton moves concomitantly with C-OMe stretch. As explained in Fig. II.12, the M06 PES has a minimum for the OMe-bound ion-pair, and a TS for C-OMe cleavage.

The two OH bound hemiacetal adducts in Fig. II.19 are conformational isomers. In **4a**-Plx-3 the methoxy group of the hemiacetal is aligned in the direction of the Fe-CO bond, and yields after proton transfer the same hemiacetaloxide product obtained by **4a**-TS-Slip-2 in Fig. II.16. This conformer is in position to undergo an outer-sphere β-hydride elimination via **4a**-TS-Slip-3 to give the metathesis products (same as in Fig. II.13). Proton transfer in **4a**-Plx-4 also leads to an octahedral hemiacetaloxide intermediate but in a conformation that points the methoxy group in the direction of the amino proton (**1a**-Fe-OHemAc-2; Fig. II.19). As mentioned in the introduction, calculations by Wang and coworkers showed C-OMe cleavage can take place from this conformation in a metal-ligand cooperation mode via **6a**-TS-MLC to give a metal-coordinated aldehyde and an alcohol that is H-bonded to the amido nitrogen (**6a**-prd-MLC; Fig. II.19).
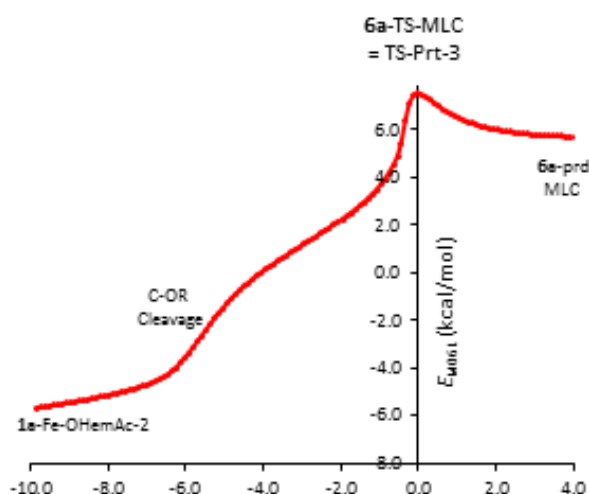
Figure II-21 IRC originating from 6a-ts-MLC described. IRC in Bohr.amu1/2 and EM06L in kcal/mol relative to the separated ester and **1a**-Fe-H.

Our IRC$_{M06L}$ calculations in Fig. II.21. confirm **6a**-TS-MLC connects **1a**-Fe-OHemAc-2 directly to **6a**-prd-MLC, but the results also reveal two distinct regions before the given TS is reached: (i) a sigmoidal region associated with C-OMe cleavage, and (ii) a region of steep energy increase due to proton transfer from the N-H bond of the ligand to the now largely dissociated OMe anion. Note that the C-OMe bond in **6a**-TS-MLC and **6a**-TS-Prd is 2.4 and 2.6 Å, respectively. In Fig. II.16. the C-OMe bond distance in the TS-OR and **5a**-Plx was 1.87 and 2.7 Å, respectively. These features strongly indicate that **6a**-TS-MLC is best perceived as a localized proton transfer step taking place after cleavage of the OR group from the hemiacetaloxide is essentially completed.

$\Delta G^{\ddagger}_{MLC}$ for alcohol "elimination" from **1a**-Fe-OHemAc-2 via **6a**-TS-MLC is 10.0 kcal/mol, significantly smaller than the corresponding $\Delta G^{\ddagger}$ for aldehyde de-insertion from **1a**-Fe-OHemAc-1 via **4a**-TS-Slip-3 (14.2 kcal/mol). However, the slippage path leads to the slightly exoergic aldehyde adduct of the metal alkoxide (**5a**-

Plx), whereas the bifunctional reaction is uphill by about 10 kcal/mol. More importantly, the computed *G* of the OMe-bound hemiacetal adduct (20.6 kcal/mol) that directly gives **5a**-Plx is lower by 2.0 kcal/mol than either OH-bound hemiacetal adduct (Fig. II. 16). The full data indicate therefore that if a free hemiacetal is formed from the reaction of the ester and **2a**-Fe-H, its fragmentation by reaction with **2a**-Fe is more likely to yield **2a**-Fe-OMe and an aldehyde than a metal coordinated aldehyde.

I.   Fragmentation by Rearrangement of 4a-Plx-1

The bifunctional route to C-OMe cleavage elucidated in Fig. 9 requires initial dissociation of the hemiacetal from adduct **4a**-Plx-1 and re-coordination into **4a**-Plx-2. Due to hydrogen bonding, the separated hemiacetal and **2**-Fe are slightly above the respective adducts. Since the given two adducts are simple conformers defined by rotation around the C-OH bond of the hemiacetal they can alternatively interchange intramolecularly while retaining the H-bond to the amide in a way similar to **4a**-TS-Slip-1. Indeed, we could identify a hemiacetal rotation TS having a geometry in which the C-H and C-OM groups are both pointed to the metal at approximately 3.0 Å (**4a**-TS-Rot; Figure II.22).

$n^{\ddagger} =$ 50i cm^{-1}

4a-Plx-1
20.0

4a-TS-Rot
23.7 kcal/mol

Slippage/Rotation within Hemiacetal Adduct.

4a-Plx-2
20.6

(7)
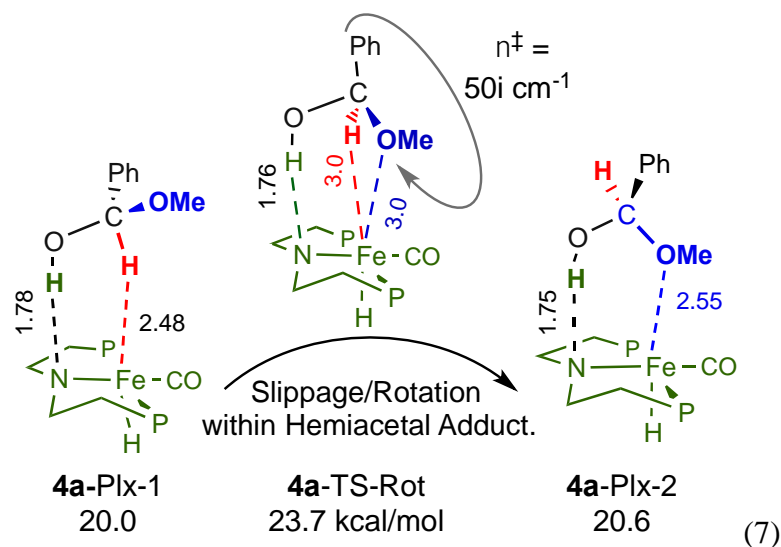
Figure II-22 Fragmentation by rearrangement of 4a-Plx-1

Not surprisingly, the imaginary frequency in **4a**-TS-Rot is only 50i cm^{-1}, implicating a very flat PES, and the rotation barrier is small: $\Delta G^{\ddagger}_{M06L} = 3.7$ kcal/mol. The absolute $G^{\ddagger}$ of **4a**-TS-Rot on the M06L/THF scale is 23.7 kcal/mol, 0.5 kcal/mole lower than **4a**-TS-Slip-1 and 2.5 kcal/mol lower than the vertical separated products. Because **4a**-plx-2 in equation 7 should undergo "spontaneous" transformation into **2a**-Fe-OMe and aldehyde, **4a**-TS-Rot provides another path for H/OR metathesis that circumvents a free hemiacetal.

J.   Conclusions

The present work addresses the nature of the C-OR cleavage step in the reaction between methyl benzoate and the octahedral hydrogenation catalyst **1**-Fe-H. We establish at first that the reaction begins in an outer sphere localized hydride transfer step leading to an ion-pair minimum (**4a**-ip-CH) and not concertedly. As summarized in

Figure II.23, from **4a**-ip-CH there are three distinct possibilities for further reaction: (i)

α-H/OR slippage of the anion to form an aldehyde and an iron-alkoxide, thus

completing a net H/OR metathesis; (ii) α-H/O⁻ ion-pair slippage that completes carbonyl

group insertion into the Fe-H bond of **1**-Fe-H; and (iii) ligand deprotonation by the

anion to make a hemiacetal.

Figure II-23 Summary of the alternative pathways for C-OR cleavage. Values in
brackets are M06L/THF Gibbs free energies in kcal/mol.

Obviously, H/OR slippage provides the least action route to C-OR cleavage. C-

OR cleavage can proceed from the insertion intermediate by a relatively low energy α-

O⁻/OR slippage that eliminates an aldehyde. To undergo C-OR cleavage the hemiacetal

has to re-coordinate to **2**-Fe in a new conformation that returns a proton to the ligand and an alkoxide to the metal. The electronic M06L/THF energies of the three TSs originating from **4a**-ip-CH are comparable, but when the ZPE, thermal and entropy terms are added the *G* values of the two slippage TSs become approximately 4 kcal/mol above TS-Prt-1. However, while the slippage route gives products that are exoergic by approximately 10 kcal/mol relative to **4a**-ip-CH, ligand deprotonation lacks any thermodynamic driving force. Thus the coordinated and dissociated hemiacetal are 1.0 and 7.2 kcal/mol, respectively, above TS-Prt-1. We even calculated a TS for hemiacetal rotation taking place over the metal while anchored to the ligand by hydrogen bond that is lower in energy than the separated hemiacetal (**4a**-TS-Rot). The DFT, solvent continuum and entropy methods used in the calculations are not expected to be equally accurate in describing the very different TSs and intermediates in Figure II.19. Nevertheless, direct ion-pair slippage requires only a trivial 1,1-rearrangement of a loosely held anion, and the free energy profiles indicate it should be at least competitive with the indirect hemiacetal route to metathesis. Furthermore, when a methanol continuum is applied in the calculations the slippage TSs are greatly stabilized relative to proton transfer, and at the ωB97X-D level they become *lower* than the hydride transfer TS, meaning the initial step of hydride transfer is the highest energy point on the ion-pair PES. The amino proton in **1**-Fe-H is probably critical in catalysis because hydrogen bonding stabilizes the ion-pair slippage TSs and not because it gives a hemiacetal. In fact, the calculations give evidence that the hydrogen bond *prevents* formation of a separated hemiacetal. Noteworthy, the methylated amino analog of

1-Fe-H where the bifunctional reaction is not applicable is an effective catalyst for CO_2 reduction. [86] When combined with results from previous calculations on Milstein's and Gusev's catalysts, the present results suggest ion-pair formation and slippage is likely to be a common reaction mode in the hydrogenation and acceptorless dehydrogenative coupling chemistry of octahedral dihydride catalysts.

CHAPTER III

HYDROGENOLYSIS: REGENERATION OF THE CATALYST

A.   Introduction

Gaining an insight about the mechanism of the regeneration is quite important. Different studies have been published regarding the regeneration of the catalyst. Hasanayn studied the H_2 Splitting by five-coordinate ruthenium complex.[84] where the coordination of the dihydrogen was preceded by breaking of the π-bond of the Ru=N. the electronic energy for this addition is negative, however the entropic effect yielded a free energy of 8.5 kcal/mol. This step is followed by a proton transfer to the nitrogen of the amide costing 10 kcal/mol of enthalpy. And the final octahedral product is favored by 4.5 kcal/mol. A summary is of this mechanism is represented in Figure III.1. Another study was done by Kirchner where he used trans-iron-PNP complex.[87] In his study he also supported the metal ligand cooperation mechanism using DFT study. As well as he tried to support his mechanism by experimental analysis where he reacted N-methylated complex with H_2 and no reaction took place.
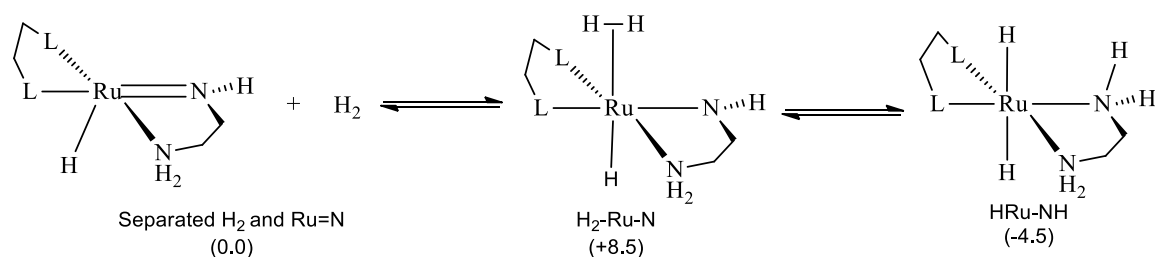
Figure III.1 Hydrogenation of the square pyramidal Ruthenium

Another possibility is considering the alkoxide formation and regenerating the catalyst. Hasanayn also studied this possibility, [84] where he suggested a concerted H_2 splitting mode across the Ru−OR bond. Since the alkoxide complex in his case was thermodynamically favored the transition state for the H_2 splitting can be considered a concerted σ-bond metathesis mode of H_2 splitting which had been implicated in hydrogenolysis of the M−C bonds of early-transition-metal complexes where the M−C bond may also have significant ionic character. [88]

Both the bifunctional and the slippage mechanisms elucidated in the previous chapter transform an ester into an aldehyde and an octahedral Iron alkoxide. For catalysis to proceed, the Iron alkoxide must react with H_2 to regenerate the iron dihydride (Figure III.2). The reaction is formally a hydrogenolysis of the Fe-OR bond.
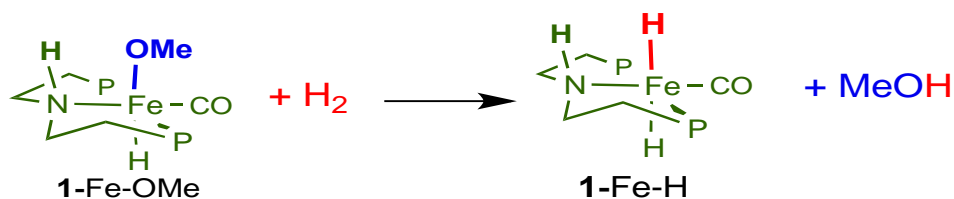
Figure III-2 hydrogenolysis of the octahedral Iron alkoxide

The calculations predict the reaction to be exoergic by 5.3 kcal/mol (ΔG = -5.3 kcal/mol), meaning catalyst regeneration is thermodynamically favorable.

B.   Discussion of the result

For catalysis, the kinetics of the given hydrogenolysis reaction will also be important. To address this question we consider one mechanism following two steps.

First, there is substitution of the alkoxide by H_2 followed by a proton transfer from the metal coordinated H_2 to the alkoxide as shown in Figure III.3. 3D displays of the two complexes are given in Figure III.4.
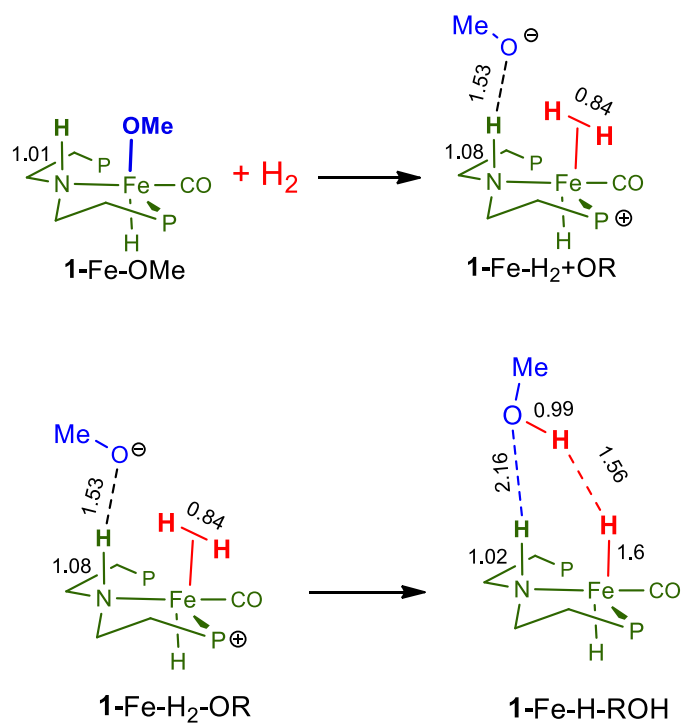
Figure III-3 Two steps for the mechansim

56
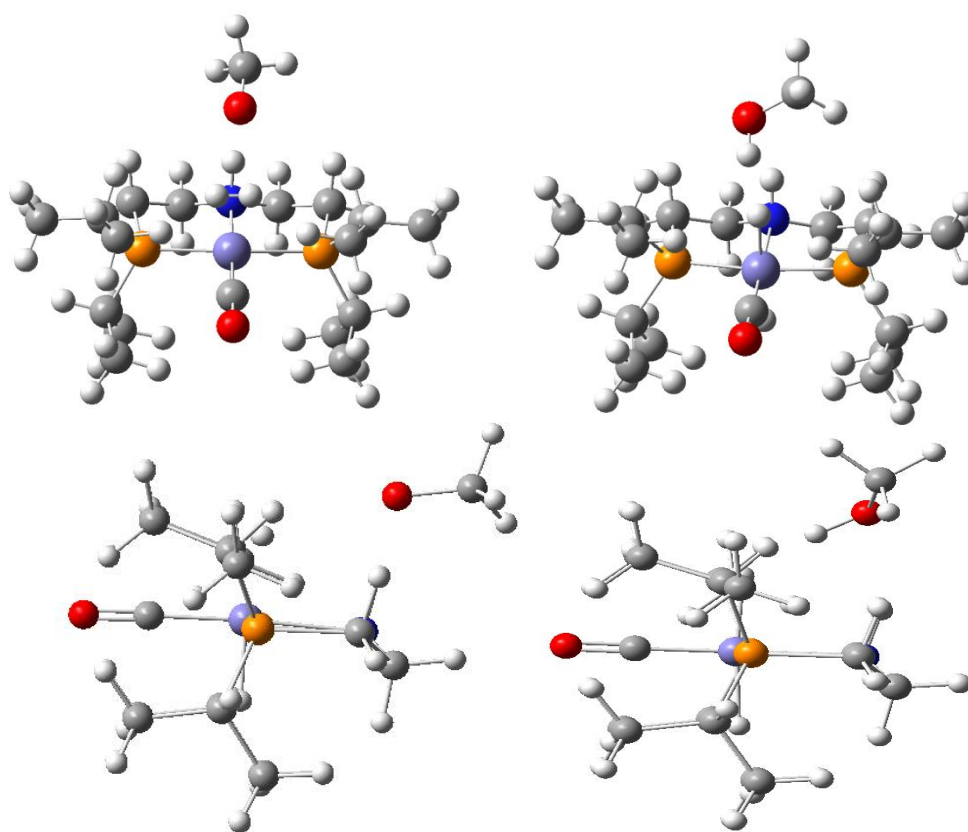
Figure III-4 The optimized 3D structure of 1-Fe-H$_2$+OR and 1-Fe-H-ROH. (With another view side by side)

The calculated dihydrogen complex from the first step has a geometry in which the H$_2$ molecule is coordinated to the metal such that it is aligned perpendicular to the N-Fe-CO axis. In the equilibrium geometry of the given intermediate, the H-H bond is stretched to 0.84 Å and the alkoxide oxygen is hydrogen bonded to the amino proton of the ligand. The NH--OR distance of 1.53 Å in the given complex implicates a rather strong H-bond, which is also an evidence in the N-H bond distance which elongates from 1.01 Å in **1**-Fe-OMe to 1.08 Å in the dihydrogen complex. Finally, because the dihydrogen complex is perpendicular to N-Fe-CO axis, the distance between the alkoxide oxygen and the dihydrogen protons is long (2.62 Å).

Dihydrogen coordination to a metal is well known to increase the acidity of H_2.[89] Thus, the second reaction involves proton transfer from the dihydrogen to the alkoxide. The reaction affords a dihydride complex to which the hydroxyl group of the alcohol is hydrogen bonded to the amino group of the ligand (1.53 Å).

The coordination of the H_2 to the complex is summarized in Figure III.5. This coordination showed to be an endothermic (ΔH=7.3 kcal/mol as well as an endoergic reaction (ΔG=13.9 kcal/mol). Although this energy may seem significant, it does not restrict the coordination of the hydrogen molecule to the complex.

1-Fe-OMe
E = 0.0; H=0.0;
S = 0.0; G= 0.0

1-Fe-H$_2$+OR
E = 4.7; H=7.3;
S = -21.8; G=13.8
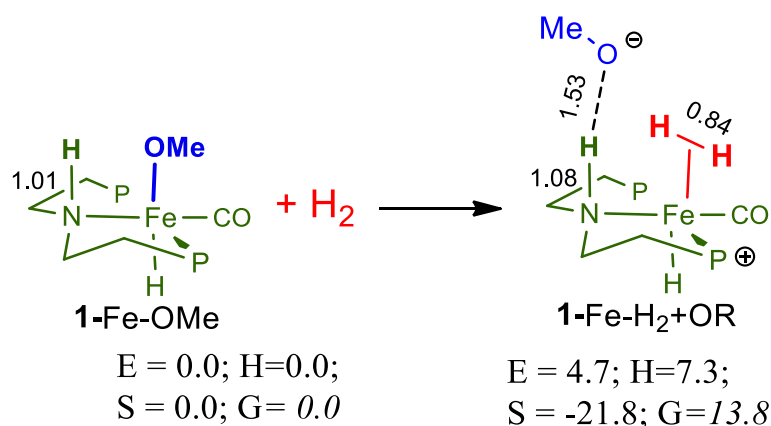
Figure III-5 Thermodynamics for the coordination of the H_2

Proton transfer from H_2 to alkoxide (Figure III.6) is computed to be highly exothermic (ΔH = -19.9 kcal/mol), which is shown to be the main component driving this reaction. The entropic factor in this reaction is slightly unfavorable ΔS= -2.7 cal.K^{-1}mol^{-1} , however, it doesn't contribute much in the reaction due to the highly exothermic nature of the reaction. Overall, the reaction is exoergic (16 kcal/mol). So after the coordination of the hydrogen molecule takes place, the splitting to favorable.
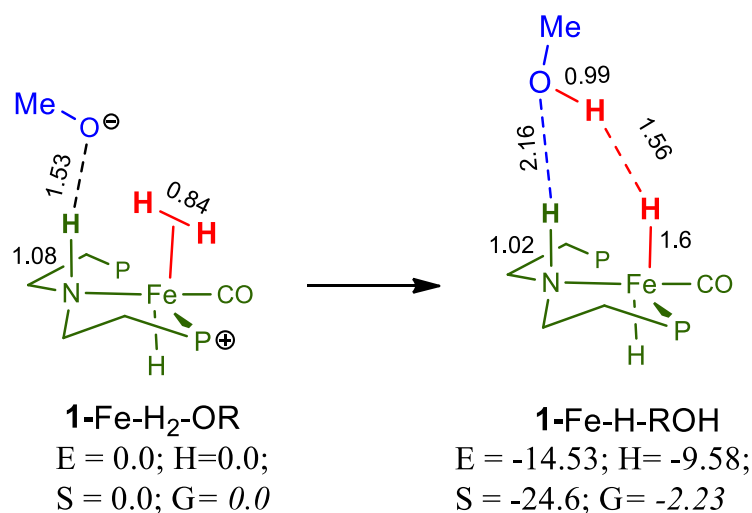
Figure III-6 Thermodynamics for the splitting of the H_2

It is important to mention here that varying the level of theory and the basis set led to minor changes in the energies. For the 1-Fe-H₂+OR, the change was 1 kcal/mol and for 1-Fe-H-ROH was about 3 kcal/mol. All the energies are tabulated in Table III.1

Table III.1 Thermodynamic Parameters for Three Intermediates with the separated products for regenerating the catalyst. (a)

	1-Fe-H2+OR	1-Fe-H-ROH	Separated Products
ΔE_{M06L}	4.7	-14.5	-6.2
ΔH_{M06L}	7.3	-9.6	-2.6
ΔS	-21.9	-24.6	9.2
ΔG_{M06L}	13.8	-2.2	-5.3
ΔG_{M06}	13.0	-5.3	-8.5
$\Delta G_{\omega B97XD}$	13.4	-5.8	-7.7

(a) In THF continuum. *G* values computed at 298K and 1 atm. Energies are given in kcal/mol/mol, entropies in cal.K⁻¹mol⁻¹

We tried to identify transition stated for the given two reactions, yet we are having difficulties in finding it. This transition state turned to be a really sensitive hard-locating one. The behavior suggests a very flat surface. Given the large thermodynamic

driving force for proton transfer, we do not expect any significant barrier for the reaction.

C.   Optimizing in methanol:

To check the effect of the solvent on the energies, we varied the polarizable solvent continuum. Here, we optimized the geometries in methanol instead of THF. The coordination showed to be less endothermic and endoergic than the calculations done in THF (H=3.9 vs 7.3 kcal/mol; G=11.0 vs 13.9 kcal/mol). The change here is around 2 kcal/mol which is insignificant to make a general conclusion regarding the solvent.

On the other hand, the proton transfer from H_2 to alkoxide is computed to be exothermic (ΔH = -11.5 kcal/mol), but less than the one computed in THF continuum (ΔH = -19.9 kcal/mol. Overall, the reaction is exoergic 11.7 kcal/mol that shows after the coordination of the hydrogen molecule, the splitting to favorable also in methanol but less favored than THF.

The separated products did not vary upon changing the solvent where the change was less than 1 kcal/mol. As we can see from table III.2, the M06 and ωB97XD functionals showed a strong agreement with the calculated energies at the lower basis set, where the difference in energies was about 2 Kcal through the three reactions.

Table III.2 Thermodynamic Parameters for Three Intermediates with the separated products for regenerating the catalyst. (a)

	Fe-H2-MeOan	FeH-NH-MeOH	Separated Products
ΔE_{M06L}	2.1	-10.5	-3.9
ΔH_{M06L}	3.9	-7.6	-2.3
ΔS	-23.9	-23.1	11.4
ΔG_{M06L}	11.0	-0.7	-5.7
ΔG_{M06}	10.4	-2.3	-7.6
ΔG_{wB97XD}	11.2	-2.1	-6.1

(a) In Methanol continuum. *G* values computed at 298K and 1 atm. Energies are given in kcal/mol/mol, entropies in cal.K^{-1}mol^{-1}

D.   Conclusion

In conclusion, Different mechanisms have been proposed for starting either from the alkoxide metal complex or from the square pyramidal one. In our study, we investigated the hydrogenation of the alkoxide complex and we identified a plausible route for the regeneration. Though we could not identify transition state for the obtained minima we believe that the suggested route is feasible. Upon changing the solvent, minor and non-concurrent changes have been showed where the difference was about 2 kcal/mol only.

CHAPTER IV

SYSTEMATIC DFT COMPARISONS OF BIFUNCTIONAL AND ION-PAIR SLIPPAGE MECHANISMS FOR C-OR BOND CLEAVAGE IN HYDROGENATION OF METHYL BENZOATE BY AN OCTAHEDRAL IRON AMINO HYDRIDE CATALYST

A. Introduction

In an attempt to study the effect of varying the nature of the ester on our calculations, we investigated the hydrogenation of methyl acetate using the Iron PNP pincer complex. Hydrogenation of methyl acetate has been studied by several groups. For example, Morris investigated the mechanism of hydrogenation using a Ruthenium Complex. [90] According to Morris, the hydrogenation is done with the bifunctional twist as we can see in Figure IV.1. This dilemma is always present when inspecting the mechanism, Metal ligand Cooperation or the Slippage. So in this Chapter we will look at the two possible mechanisms and identify the lower energy route.
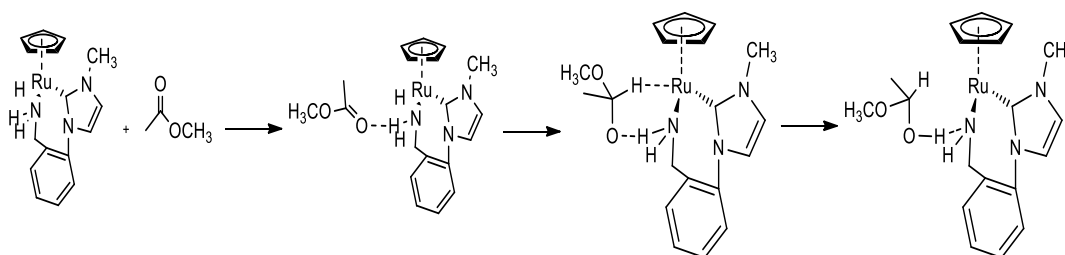
Figure IV-1 Bifunctional addition of a hydride/proton pair across the carbonyl group of methyl acetate starting from the hydride complex

B. Thermodynamics of the Reactions

In this Chapter, we will also study the three reactions that are relevant to our study. The three reactions are represented in figure IV.2: bifunctional hydrogenation (eq 1), H/OR metathesis (eq 2) and carbonyl group insertion (eq 3)
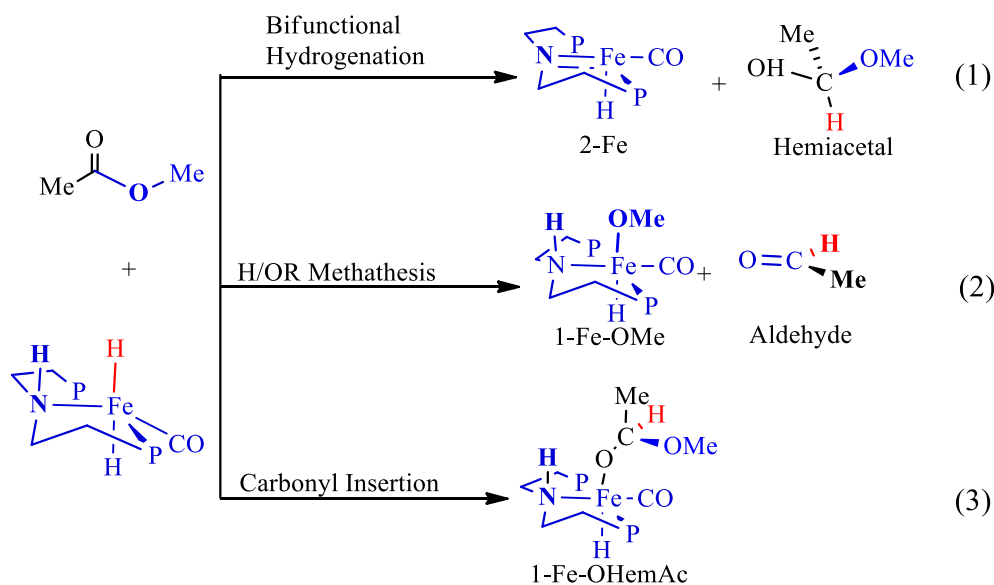
Figure IV-2 Three reactions between 1-Fe-H and methyl acetate

We considered here the most favored conformational structures. Therefore, for these structures we calculated the thermodynamics of these reactions and tabulated in Table III.1. At the M06L, the products of the Slippage mechanism (the aldehyde and the alkoxide complex) seemed to have the lowest free energy with 4.7 kcal/mol, which is lower than the hemiacetal products that cost 24.7 kcal/mol and that of carbonyl insertion the lies between them by having a free energy of 7.6 kcal/mol. These energies were influenced by the enthalpy values of each reaction. As we can see that the MLC mechanism tends to a be highly endothermic reaction by 25.3 kcal/mol, which is higher than the metathesis (4.9 kcal/mol). On the other hand, the insertion is slightly exothermic by -0.1 kcal/mol. As for the entropy, it plays a less decent role in favoring one path on the other; though the bifunctional hydrogenation has the highest entropy

value by 4.0 cal.K^{-1}mol^{-1}, it falls in the last between the three reactions in term of free energy. To make sure that these numbers provide a reliable conclusion, we did single point calculations on higher basis set and using different functionals. The M06 functional showed a good agreement with M06L where the slippage mechanism is more favored than the insertion by 1 kcal/mol, and the bifunctional mechanism still has the highest energy barrier upon them by 22.0 kcal/mol. Interestingly, at the ωB97X-D showed that the carbonyl insertion is slightly more favored than the metathesis, 5.6 vs 6.3 kcal/mol respectively, and in consistency with the other results, the bifunctional hydrogenation was the highest by 22.5 kcal/mol.

Table IV.1 Thermodynamic Parameters for Three Reactions Between 1-Fe-H and methyl acetate Defined in Figure IV.2 [a]

	Bifunctional Hydrogenation (eq 4)	H/OR Metathesis (eq 5)	Carbonyl Insertion (eq 6)
ΔE_{M06L}	23.5	3.9	-4.0
ΔH_{M06L}	25.3	4.9	-.0.1
$\Delta S(scaled)$	4.0	2.5	-21.0
ΔG_{M06L}	24.7	4.7	7.6
ΔG_{M06}	22.0	8.1	9.0
ΔG_{wB97XD}	22.5	6.3	5.6

(a) In THF continuum. G values computed at 298K and 1 atm.

Energies are given in kcal/mol, entropies in cal.K^{-1}mol^{-1}

C. Bifunctional Hemiacetal Formation

64

The PES for the reaction between 1a-Fe-H and methyl acetate (3') is represented in figure IV.3. First, we identified a pre-complex of these two molecules described by a distance of 1.47 Å between the hydride of the metal and the carbonyl of the ester. The electronic energy of this complex is -7.4 kcal/mol. Comparable energies are computed at the M06 (-6.0 kcal/mol) and ωB97X-D (-6.9 kcal/mol) levels. It is worth mentioning here that based on the geometric parameters in **3a**'-Plx, there is a strong hydrogen bonding between the hydrogen of the amino proton and the carbonyl oxygen. This complex appeared to have almost the same free energy when the methyl benzoate, where they differ by 1 kcal/mol only.
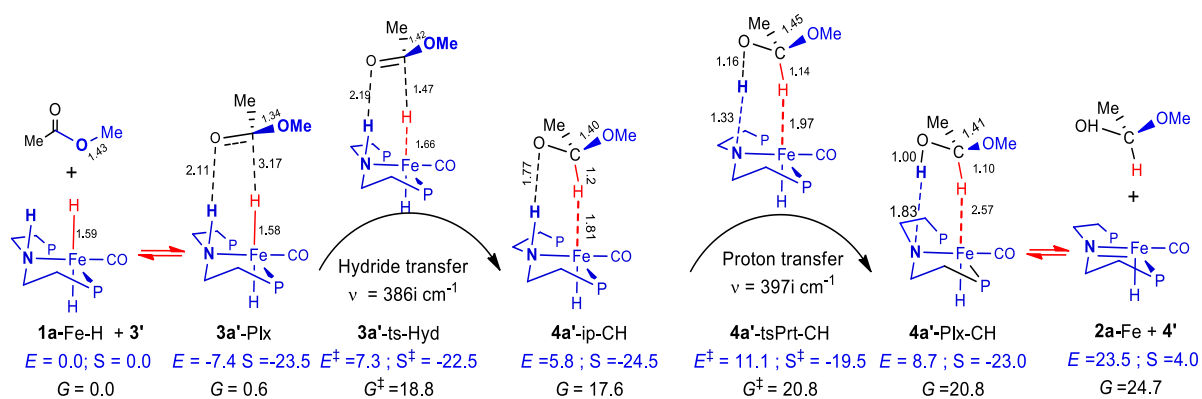
Figure IV-3PES for hemiacetal formation from 1a-Fe-H and 3. M06L/def2/THF results in kcal/mol and Å.

A transition state for a localized hydride transfer from the metal to the carbonyl was detected, forming an ion-pair minimum (4a'-ip-CH). The 3D structure for this transition state is shown in Figure IV.4. This transfer costs 18.8 kcal/mol of Gibbs free energy with an electronic barrier of 7.3 kcal/mol, both parameters give a high-energy barrier and comparable with that obtained with the methyl benzoate 17.3 and 10.1 kcal/mol respectively.
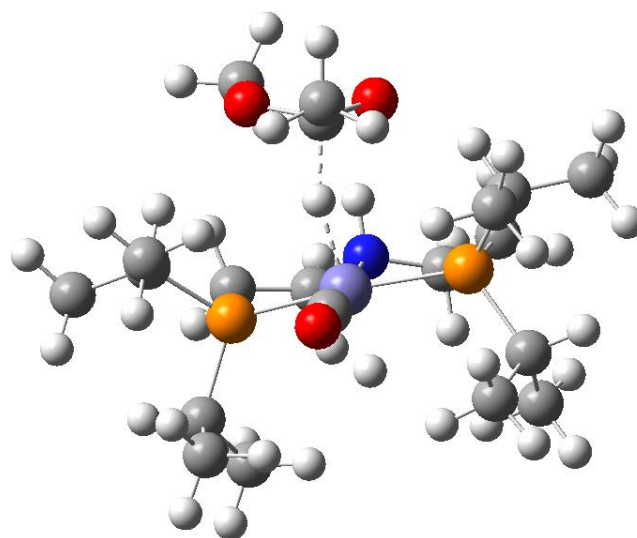
Figure IV-4 3D structure for the hydride transition state

The bifunctional taste relies on the interference of the ligand in this mechanism, for this case we succeeded in locating a proton transfer from the nitrogen to the oxygen of the carbonyl (**4a'**-ts-Prt-1). This step is considered to be the rate determining step by having the highest energy needed (20.8 kcal/mol) which differs in 2 kcal/mol when compared with methyl benzoate (19.0 kcal/mol). This step leads to a hemiacetal pre-complex which is also at a high energy 20.8 kcal/mol higher than the Proton transfer by 3 kcal/mol. Finally, obtaining the separated products (hemiacetal and 2a'-Fe) cost 24.7 kcal/mol of free energy. As we can see, there is no driving force for the reaction to take this pathway of the reaction.
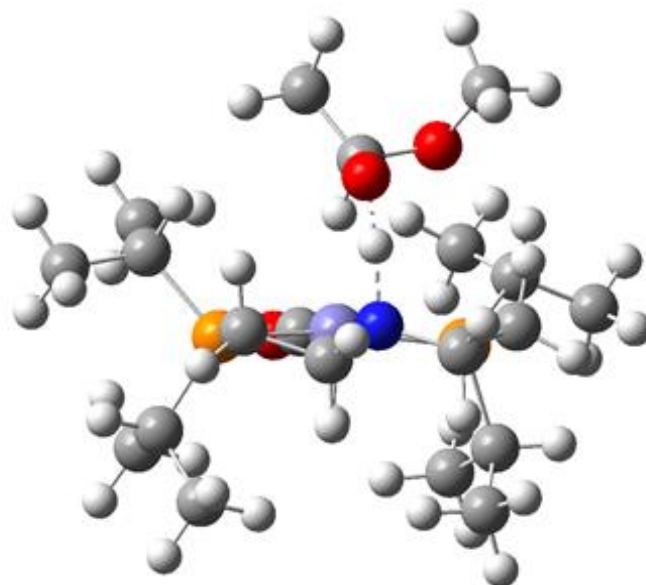
Figure IV-5 3D structure for the proton transition state

Upon changing the polarizable continuum to methanol instead of THF we noticed that there are no major changes in the energies obtained in the remarkable steps for the MLC path, however the full data is tabulated in table IV.2. The Proton transfer decreased by 0.4 kcal/mol (20.8 vs 20.4 kcal/mol), which is insignificant difference. As for the separated products, the hemiacetal and the five-coordinated products, there is no effect for the solvent. The free energies were almost identical, 23.7 kcal/mol and 23.3 kcal/mol.

Table IV.2 Comparison for thermodynamic parameters for the bifunctional mechanism key steps in two different solvents (a)

Bifunctional Mechanism	Proton Transfer Methanol	Proton Transfer THF	Separated products Methanol	Separated products THF
ΔE_{M06L}	9.8	11.1.	21.7	23.5
ΔH_{M06L}	12.5	10.7	24.2	25.3
ΔS (scaled)	-14.0	-19.0	3.0	4.0
ΔG_{M06L}	20.4	20.8	23.3	24.7
ΔG_{M06}	18.3	19.1	20.5	22.0
ΔG_{wB97XD}	15.2	17.7	20.9	22.5

(a) G values computed at 298K and 1 atm.

Energies are given in kcal/mol, entropies in cal.$K^{-1}mol^{-1}$

D. H/OR Metathesis via Ion-Pair Slippage

Another path has been identified that showed to have a lower energy. In the proposed mechanism, we agree on the hydride transfer to be the first step in the mechanism, common with the MLC one. After the formation of the ion-pair complex, we identified a new plausible path that can be called a direct ion-pair H/OR slippage mode. Same to the proposed slippage of for the methyl benzoxide, we identified a slippage transition state for the methyl ethoxide.
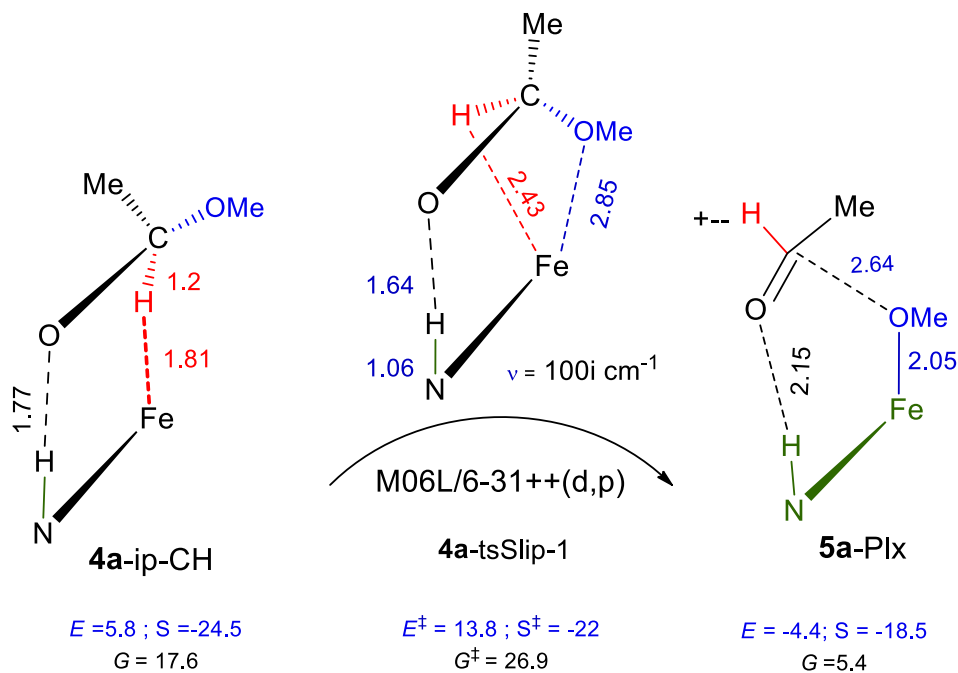
Figure IV-6 Ion-pair slippage completing H/OR metathesis. Energies in kcal/mol relative to the separated 3' and 2a-Fe-H.

The founded TS maintains a strong hydrogen bond between the terminal oxygen of the anion and the amino proton of the ligand (NH-O= 1.64 Å). It was observed that as the rotation takes place the distance between the metal and the transferred hydride increases from 1.81 to 2.43 while the Fe--OMe distance decreases from 3.41 to 2.85Å. A 3D image for the TS is represented in Figure IV.7; and it is important to mention that the imaginary frequency of this TS is slightly higher than that obtained with the methyl benzoate (85i cm^{-1} to 100i cm^{-1}).
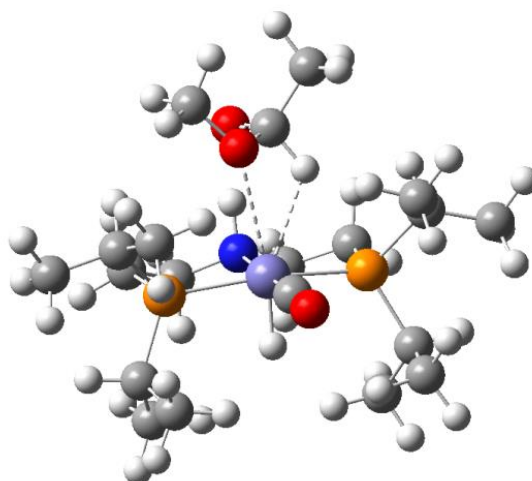
Figure IV-7 3D structure for the slippage transition state.

From a thermodynamic point of veiw, Figure IV.8 represent the full reaction

mechansim for the slippage mechanism. The slippage step tends to have a higher energy

than the proton transfer in the MLC mechanism (20.8 kcal/mol vs 26.9 kcal/mol). The 6

kcal/mol difference may suggest that the bifunctional route is the predominnat one. But,

if we look at the next step of each mechanism, we can see that the hemiactal complex in

the MLC mechanism is 16 kcal/mol higher than the aldehyde complex formed by the

slippage one, (20.8 kcal/mol vs 5.4 kcal/mol). The same significance is present when

comparing the separated product of each path, the slippage path is favored by 16

kcal/mol (20.8 vs 4.7 kcal/mol) which can be conclusive towards the direct H/OR

methathesis.
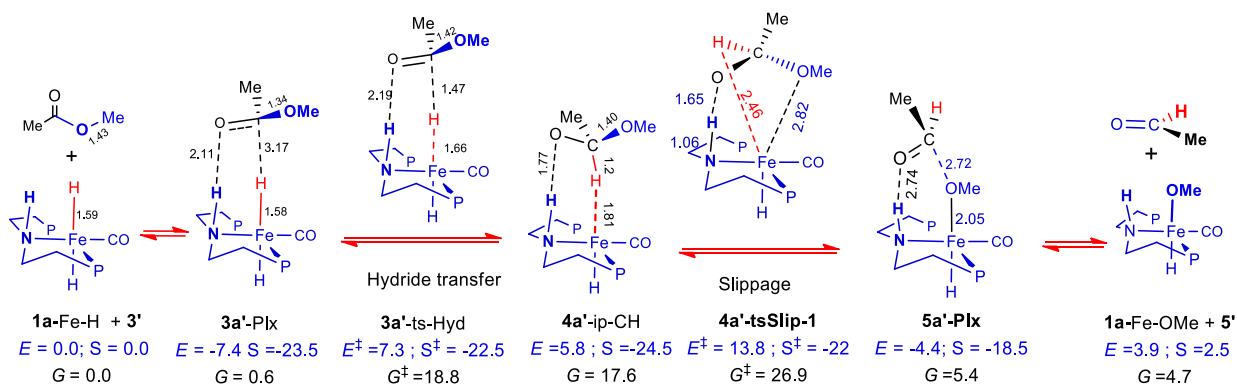
Figure IV-8 PES for hemiacetal formation from 1a-Fe-H and 3. M06L/def2/THF results in kcal/mol and Å.

In comparison with the data obtained in the hydrogenation of methyl benzoate, the slippage step seemed to be higher in energy in the methyl acetate slippage by 2.7 kcal/mol. And this difference was the same at the end of the mechansim where the separated products of both reactions were 2.4 and 4.7 kcal/mol for methyl benzoate and methyl acetate, respectively.

Changing the polarizable continuum to methanol led to a major changes in the energies for the key steps in the mechanism that are summarized in table IV.3. The slippage transtion state decreased dramatically by 8 kcal/mol to have approximately the same cost as the proton transfer (20.4 kcal/mol). And the separted products are slightly more favored by 1 kcal/mol in the methanol than THF and 19 kcal/mol more favored than the separated products of the MLC.

Table IV.3 Comparison for thermodynamic parameters for the Slippage mechanism key steps in two different solvents (a)

H/OR Metathesis	Slippage Methanol	Slippage THF	Separated products Methanol	Separated products THF
ΔE_{M06L}	5.4	13.8	1.8	3.9
ΔH_{M06L}	11.5	16.5	3.8	4.9
ΔS	-22	-22	3.1	2.5
ΔG_{M06L}	20.1	26.9	3.7	4.7
ΔG_{M06}	20.4	28.0	6.7	8.1
ΔG_{wB97XD}	16.1	24.6	4.4	6.3

(a) G values computed at 298K and 1 atm.

Energies are given in kcal/mol, entropies in cal.K^{-1}mol^{-1}

E. PES for H/OR Metathesis via Carbonyl Insertion and De-insertion

Another variation for the slippage route is to consider the carbonyl insertion and de-insertion, where the anionic oxygen of the hemiacetaloxide becomes coordinated to the metal as represented in figure IV.9. Rotation followed by de-insertion of the anionic oxygen and coordination of the methyl oxide to the iron center lead to the formation of the direct metathesis products as an indirect route. The thermodynamic of this insertion is represented in Figure IV-9. As we can see, this insertion is less favored than the H/OR slippage by 3 kcal/mol (4.7 vs 7.6 kcal/mol). However, de-insertion can take us back to the products of the direct metathesis as an indirect route. Single point calculations have also been done at higher basis set and different functionals; we

noticed a decent agreement with the calculations done at smaller basis set at M06L level of theory.
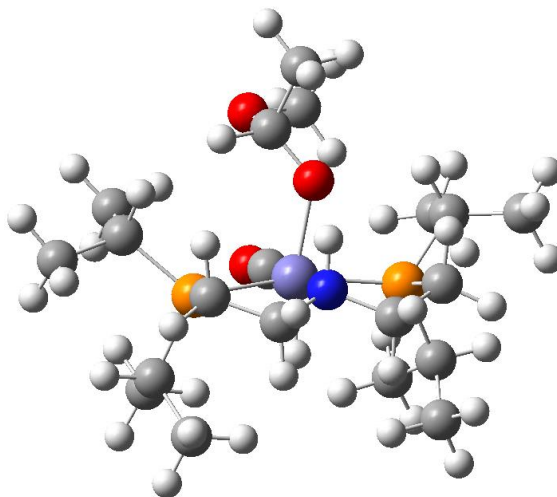
Figure IV-9 3D structure for the Insertion Product.

In comparison with the insertion done for methyl benzoate; we can see that the obtained free energy is less favored than that by 11 kcal/mol (4.0 vs 15.7 kcal/mol). Although the free Energy increased, the insertion step still bears an intermediate energy among the possible routes. We also studied the role of the polarizable solvent, so we optimized the geometries in Methanol instead of THF and checked the energies. We found that it becomes slightly more favored in Methanol by 2.7 kcal/mol of free energy.
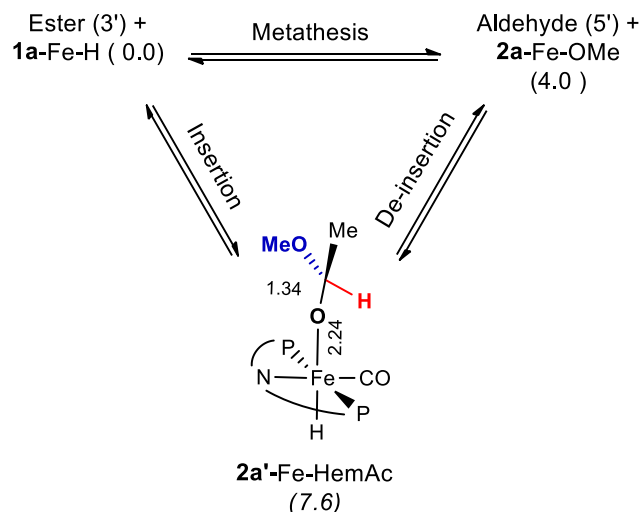
Figure IV-10 3D H/OR metathesis via carbonyl group insertion and de-insertion

F. Conclusion:

Summing up all these observations, Gibbs free energy profiles are done to compare the hemiacetal and the aldehyde formations at different functionals levels as well as studying the effect of the two solvents, THF and Methanol. As a clear image can be visualized that the Slippage mechanism in any path it follows, will be the more favored route for ester hydrogenation by the Iron PNP complex. Moreover, we can assure for an important role of the solvent in affecting the energies in the calculations.
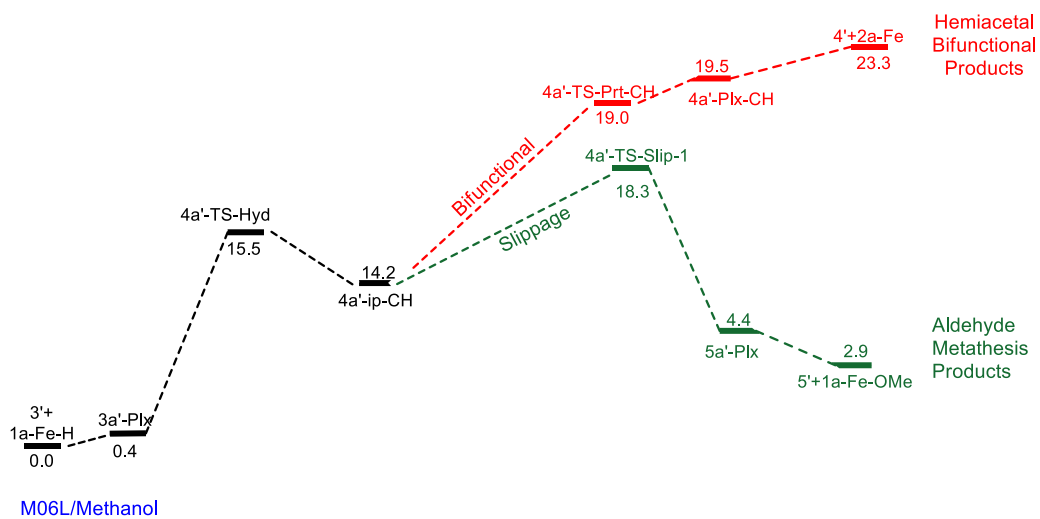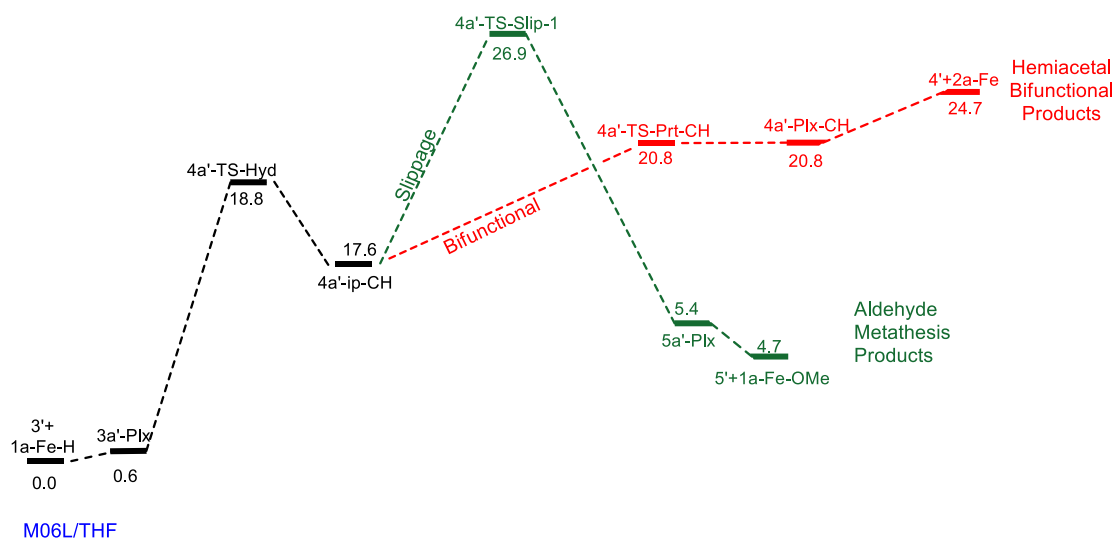
Figure IV-11 Gibbs free energy profiles for hemiacetal and aldehyde formation from **1a**-Fe-H and **3'** (at 298 K and 1 atm in kcal/mol,)

CHAPTER V

CONCLUSION

In conclusion, science is trying to make chemical processes more sustainable and as green as possible. This is done be reducing the amount of toxic compounds produced or even eliminating them. In the same domain and moving into more nature-friendly, esterification reaction has shifted from the use of toxic metals that produce harmful waste into a greener way that is also efficient.

We considered an octahedral iron complex that is used to hydrogenate esters and produce alcohols. In specific, we were after investigating the mechanism of this catalyst and this was done using electronic structure DFT methods. So we compared the pathway of the well-known and accepted mechanism so far, the metal ligand cooperation, with the proposed mechanism, the slippage one.

The newly identified route is a more direct, low energy route for the ester hydrogenation that can be summarized as a direct metathesis. This new path involves the formation of an ion pair that undergoes simple rearrangement to yield iron alkoxide and an aldehyde.

In the same context, we studied the effect of varying the ester molecule on the pathway of the hydrogenation. We found that changing the ester from methyl benzoate to methyl acetate has a significant effect on the energies. The energies change considerably, where the benzoate ester shows to have a lower energy barrier than that of

the methyl in both, the MLC and the Slippage mechanisms. In both cases, the Slippage pathway showed to be the more favored path, regardless of the nature of the ester.

Moreover, in this work we studied the regeneration of the catalyst. We identified three intermediates that could lead to the octahedral catalyst, yet we could not identify a transition state to plot a convincing mechanism. On the other hand, the suggested mechanism could also be plausible after identifying and linking the intermediates to get a reasonable mechanism.

This study paves the way to reconsidering the Metal-Ligand Cooperation mechanism that has been thought of to be as a generally accepted mechanism and to start pointing out more direct metathesis mechanisms that do not involve the modification of the ligand or part of it. Moreover, several catalysts are being developed and they are based on the metal ligand cooperation to explain the mechanisms of these systems. On the other hand, considering a newly proposed mechanism could be helpful in directing the mechanistic studies into more vivid conclusions.

In the future, we should consider using these catalysts in the industries. The shift from the ruthenium and other costly metals is important in saving not only money but also nature. Even though most of these metals are mined from undeveloped countries, we do not have to damage Africa to benefit other countries. So more work must be done to make sure which mechanism is the correct one. Experimental analyses are needed to be accompanied with any theoretical work to insure which mechanism can best fit this catalysis

References

1. Sabatier, P. and J. Sendrens, *Action of hydrogen on acetylene in presence of nickel.* Comptes Rendus Hebdomadais des Seances de l'Academie des science, 1899. **128**: p. 1173.
2. Sabatier, P., *The method of direct hydrogenation by catalysis. nobel lecture, december 11, 1912. nobel lectures in chemistry 1901-1921.* 1966, Elsevier Publishing Company, Amsterdam.
3. Bancroft, W.D. and A.B. George, *Hydrogenation of benzene with nickel and platinum.* The Journal of Physical Chemistry, 1931. **35**(8): p. 2219-2225.
4. Osborn, J.A., et al., *The preparation and properties of tris (triphenylphosphine) halogenorhodium (I) and some reactions thereof including catalytic homogeneous hydrogenation of olefins and acetylenes and their derivatives.* Journal of the Chemical Society A: Inorganic, Physical, Theoretical, 1966: p. 1711-1732.
5. Blum, Y., et al., *(Cyclopentadienone) ruthenium carbonyl complexes-a new class of homogeneous hydrogenation catalysts.* Organometallics, 1985. **4**(8): p. 1459-1461.
6. Crabtree, R.H. and M.W. Davis, *Directing effects in homogeneous hydrogenation with [Ir (cod)(PCy3)(py)] PF6.* The Journal of Organic Chemistry, 1986. **51**(14): p. 2655-2661.
7. Candlin, J. and A. Oldham, *Selective hydrogenation of unsaturated carbon-carbon bonds with rhodium complexes.* Discussions of the Faraday Society, 1968. **46**: p. 60-71.
8. O'Connor, C. and G. Wilkinson, *Selective homogeneous hydrogenation of alk-1-enes using hydridocarbonyltris (triphenylphosphine) rhodium (I) as catalyst.* Journal of the Chemical Society A: Inorganic, Physical, Theoretical, 1968: p. 2665-2671.
9. Jourdant, A., E. González-Zamora, and J. Zhu, *Wilkinson's catalyst catalyzed selective hydrogenation of olefin in the presence of an aromatic nitro function: a remarkable solvent effect.* The Journal of organic chemistry, 2002. **67**(9): p. 3163-3164.
10. Knowles, W.S. and M.J. Sabacky, *Catalytic asymmetric hydrogenation employing a soluble, optically active, rhodium complex.* Chemical Communications (London), 1968(22): p. 1445-1446.
11. Horner, L., H. Siegel, and H. Büthe, *Asymmetric catalytic hydrogenation with an optically active phosphinerhodium complex in homogeneous solution.* Angewandte Chemie International Edition in English, 1968. **7**(12): p. 942-942.
12. Dang, T. and H. Kagan, *The asymmetric synthesis of hydratropic acid and amino-acids by homogeneous catalytic hydrogenation.* Journal of the Chemical Society D: Chemical Communications, 1971(10): p. 481-481.
13. Ohkuma, T., et al., *Preferential hydrogenation of aldehydes and ketones.* Journal of the American Chemical Society, 1995. **117**(41): p. 10417-10418.

14.	Yamakawa, M., H. Ito, and R. Noyori, *The metal-ligand bifunctional catalysis: A theoretical study on the ruthenium (II)-catalyzed hydrogen transfer between alcohols and carbonyl compounds.* Journal of the American Chemical Society, 2000. **122**(7): p. 1466-1478.

15.	Adkins, H. and K. Folkers, *The catalytic hydrogenation of esters to alcohols.* Journal of the American Chemical Society, 1931. **53**(3): p. 1095-1097.

16.	Connor, R., K. Folkers, and H. Adkins, *The preparation of copper-chromium oxide catalysts for hydrogenation.* Journal of the American chemical society, 1932. **54**(3): p. 1138-1145.

17.	Folkers, K. and H. Adkins, *The Catalytic Hydrogenation of Esters to Alcohols. II.* Journal of the American Chemical Society, 1932. **54**(3): p. 1145-1154.

18.	Brands, D., et al., *Sulfur deactivation of fatty ester hydrogenolysis catalysts.* Journal of Catalysis, 1999. **186**(1): p. 169-180.

19.	Huang, H., G. Cao, and S. Wang, *An evaluation of alkylthiols and dialkyl disulfides on deactivation of Cu/Zn catalyst in hydrogenation of dodecyl methyl ester to dodecanol.* Journal of Industrial and Engineering Chemistry, 2014. **20**(3): p. 988-993.

20.	Deshpande, V., K. Ramnarayan, and C.S. Narasimhan, *Studies on ruthenium-tin boride catalysts II. Hydrogenation of fatty acid esters to fatty alcohols.* Journal of Catalysis, 1990. **121**(1): p. 174-182.

21.	Zhou, Y., et al., *Hydrogenation of methyl propionate over Ru–Pt/AlOOH catalyst: Effect of surface hydroxyl groups on support and solvent.* Catalysis Communications, 2009. **11**(2): p. 137-141.

22.	Wittstock, A., et al., *Nanoporous gold catalysts for selective gas-phase oxidative coupling of methanol at low temperature.* Science, 2010. **327**(5963): p. 319-322.

23.	Dhillon, R.S., *Synthesis of esters.* hydroboration and organic synthesis: 9-Borabicyclo [3.3. 1] nonane (9-BBN), 2007: p. 241-252.

24.	Fischer, C.F., *General hartree-fock program.* Computer physics communications, 1987. **43**(3): p. 355-365.

25.	Clarke, M.L., *Recent developments in the homogeneous hydrogenation of carboxylic acid esters.* Catalysis Science & Technology, 2012. **2**(12): p. 2418-2423.

26.	Pritchard, J., et al., *Heterogeneous and homogeneous catalysis for the hydrogenation of carboxylic acid derivatives: history, advances and future directions.* Chemical Society Reviews, 2015. **44**(11): p. 3808-3833.

27.	Morales-Morales, D., *Pincer complexes. Applications in catalysis.* Rev. Soc. Quim. Mex, 2004. **48**: p. 338-346.

28.	Chakraborty, S., W.W. Brennessel, and W.D. Jones, *A molecular iron catalyst for the acceptorless dehydrogenation and hydrogenation of N-heterocycles.* Journal of the American Chemical Society, 2014. **136**(24): p. 8564-8567.

29.	zell, t., y. ben-david, and d. milstein, *Unprecedented iron‑catalyzed eester hydrogenation. mild, selective, and efficient hydrogenation of trifluoroacetic esters to alcohols catalyzed by an iron pincer complex.* Angewandte Chemie, 2014. **126**(18): p. 4773-4777.

30.	Werkmeister, S., et al., *Hydrogenation of esters to alcohols with a well‑defined iron complex.* Angewandte Chemie International Edition, 2014. **53**(33): p. 8722-8726.

31.   Chakraborty, S., et al., *Iron-based catalysts for the hydrogenation of esters to alcohols.* Journal of the American Chemical Society, 2014. **136**(22): p. 7869-7872.

32.   Dub, P.A. and T. Ikariya, *Catalytic reductive transformations of carboxylic and carbonic acid derivatives using molecular hydrogen.* ACS Catalysis, 2012. **2**(8): p. 1718-1741.

33.   Khusnutdinova, J.R. and D. Milstein, *Metal–ligand cooperation.* Angewandte Chemie International Edition, 2015. **54**(42): p. 12236-12273.

34.   Sues, P.E., K.Z. Demmans, and R.H. Morris, *Rational development of iron catalysts for asymmetric transfer hydrogenation.* Dalton Transactions, 2014. **43**(21): p. 7650-7667.

35.   Sui-Seng, C., et al., *Highly efficient catalyst systems using iron complexes with a tetradentate PNNP ligand for the asymmetric hydrogenation of polar bonds.* Angewandte Chemie, 2008. **120**(5): p. 954-957.

36.   Meyer, N., A.J. Lough, and R.H. Morris, *Iron (II) complexes for the efficient catalytic asymmetric transfer hydrogenation of ketones.* Chemistry–A European Journal, 2009. **15**(22): p. 5605-5610.

37.   Mikhailine, A.A. and R.H. Morris, *Effect of the structure of the diamine backbone of P− N− N− P ligands in iron (II) complexes on actalytic activity in the transfer hydrogenation of acetophenone.* Inorganic chemistry, 2010. **49**(23): p. 11039-11044.

38.   Lagaditis, P.O., A.J. Lough, and R.H. Morris, *Low-valent ene–amido iron complexes for the asymmetric transfer hydrogenation of acetophenone without base.* Journal of the American Chemical Society, 2011. **133**(25): p. 9662-9665.

39.   Mikhailine, A.A., M.I. Maishan, and R.H. Morris, *Asymmetric transfer hydrogenation of ketimines using well-defined iron (II)-based precatalysts containing a PNNP ligand.* Organic letters, 2012. **14**(17): p. 4638-4641.

40.   Lagaditis, P.O., A.J. Lough, and R.H. Morris, *Iron complexes for the catalytic transfer hydrogenation of acetophenone: steric and electronic effects imposed by alkyl substituents at phosphorus.* Inorganic chemistry, 2010. **49**(21): p. 10057-10066.

41.   Zuo, W., et al., *Iron catalysts containing amine (imine) diphosphine P-NH-NP ligands catalyze both the asymmetric hydrogenation and asymmetric transfer hydrogenation of ketones.* Organometallics, 2014. **33**(20): p. 5791-5801.

42.   Prokopchuk, D.E., et al., *Spectroscopic and DFT study of ferraaziridine complexes formed in the transfer hydrogenation of acetophenone catalyzed using trans-[Fe (CO)(NCMe)(PPh₂C₆H₄CH-NCH₂−) ₂-κ4 P, N, N, P](BF₄) 2.* Organometallics, 2012. **31**(8): p. 3056-3064.

43.   Prokopchuk, D.E. and R.H. Morris, *Inner-sphere activation, outer-sphere catalysis: Theoretical study on the mechanism of transfer hydrogenation of ketones using iron (II) PNNP eneamido complexes.* Organometallics, 2012. **31**(21): p. 7375-7385.

44.   Zell, T., et al., *Iron dicarbonyl complexes featuring bipyridine-based pnn pincer ligands with short interpyridine C- C bond lengths: Innocent or non-innocent ligand?* Chemistry–A European Journal, 2014. **20**(15): p. 4403-4413.

45. Gunanathan, C. and D. Milstein, *Metal–ligand cooperation by aromatization–dearomatization: a new paradigm in bond activation and "green" catalysis.* Accounts of chemical research, 2011. **44**(8): p. 588-602.

46. Zell, T., et al., *Synthesis, structures, and dearomatization by deprotonation of iron complexes featuring bipyridine-based PNN pincer ligands.* Inorganic chemistry, 2013. **52**(16): p. 9636-9649.

47. van der Vlugt, J.I. and J.N. Reek, *Neutral tridentate PNP ligands and their hybrid analogues: Versatile non‐innocent scaffolds for homogeneous Catalysis.* Angewandte Chemie International Edition, 2009. **48**(47): p. 8832-8846.

48. Poverenov, E. and D. Milstein, *Noninnocent behavior of PCP andPCN pincer ligands of late metal complexes*, in *organometallic pincer chemistry.* 2013, Springer. p. 21-47.

49. Zhang, J., et al., *Iron (II) complexes based on electron-rich, bulky PNN-and PNP-type ligands.* Inorganica chimica acta, 2006. **359**(6): p. 1955-1960.

50. Trovitch, R.J., E. Lobkovsky, and P.J. Chirik, *Bis (diisopropylphosphino) pyridine iron dicarbonyl, dihydride, and silyl hydride complexes.* Inorganic chemistry, 2006. **45**(18): p. 7252-7260.

51. Pelczar, E.M., et al., *Unusual structural and spectroscopic features of some PNP-pincer complexes of iron.* Organometallics, 2008. **27**(22): p. 5759-5767.

52. Langer, R., et al., *Low‐pressure hydrogenation of carbon dioxide catalyzed by an iron pincer complex exhibiting noble metal activity.* Angewandte Chemie International Edition, 2011. **50**(42): p. 9948-9952.

53. Langer, R., et al., *Efficient hydrogenation of ketones catalyzed by an iron pincer complex.* Angewandte Chemie, 2011. **123**(9): p. 2168-2172.

54. Langer, R., et al., *Iron borohydride pincer complexes for the efficient hydrogenation of ketones under mild, base‐free conditions: synthesis and mechanistic insight.* Chemistry–A European Journal, 2012. **18**(23): p. 7196-7209.

55. Zell, T., Y. Ben-David, and D. Milstein, *Highly efficient, general hydrogenation of aldehydes catalyzed by PNP iron pincer complexes.* Catalysis Science & Technology, 2015. **5**(2): p. 822-826.

56. Hasanayn, F. and A. Baroudi, *Direct H/OR and OR/OR' metathesis pathways in ester hydrogenation and transesterification by milstein's catalyst.* Organometallics, 2013. **32**(9): p. 2493-2496.

57. Takebayashi, S., et al., *Experimental investigations of a partial Ru–O bond during the metal–ligand bifunctional addition in noyori-type enantioselective ketone hydrogenation.* Journal of the American Chemical Society, 2011. **133**(25): p. 9666-9669.

58. Chakraborty, S., et al., *Well-defined iron catalysts for the acceptorless reversible dehydrogenation-hydrogenation of alcohols and ketones.* ACS Catalysis, 2014. **4**(11): p. 3994-4003.

59. Wiberg, K.B., K.M. Morgan, and H. Maltz, *Thermochemistry of carbonyl reactions. 6. A study of hydration equilibria.* Journal of the American Chemical Society, 1994. **116**(24): p. 11067-11077.

60. Qu, S., et al., *Computational mechanistic study of Fe-catalyzed hydrogenation of esters to alcohols: improving catalysis by accelerating precatalyst activation with a lewis base.* ACS Catalysis, 2014. **4**(12): p. 4377-4388.

61. Li, H., et al., *Computational study on the catalytic role of pincer ruthenium (II)-PNN complex in directly synthesizing amide from alcohol and amine: the origin of selectivity of amide over ester and imine.* Organometallics, 2011. **30**(19): p. 5233-5247.

62. Baroudi, A., et al., *Calculation of ionization energy, electron affinity, and hydride affinity trends in pincer-ligated d8-Ir (^{t}Bu$_4$PXCXP) complexes: implications for the thermodynamics of oxidative H$_2$ addition.* Inorganic chemistry, 2014. **53**(23): p. 12348-12359.

63. Gunanathan, C. and D. Milstein, *Bond activation and catalysis by ruthenium pincer complexes.* Chemical Reviews, 2014. **114**(24): p. 12024-12087.

64. Hasanayn, F., et al., *Hydrogenation of dimethyl carbonate to methanol by trans-[Ru(H)$_2$(PNN)(CO)] catalysts: DFT evidence for ion-pair-mediated metathesis paths for C–OMe bond cleavage.* Organometallics, 2013. **32**(23): p. 6969-6985.

65. Chen, X., Y. Jing, and X. Yang, *Unexpected direct hydride transfer mechanism for the hydrogenation of ethyl acetate to ethanol catalyzed by SNS Pincer ruthenium complexes.* Chemistry–A European Journal, 2016. **22**(6): p. 1950-1957.

66. Bielinski, E.A., et al., *Lewis acid-assisted formic acid dehydrogenation using a pincer-supported iron catalyst.* Journal of the American Chemical Society, 2014. **136**(29): p. 10234-10237.

67. Lange, S., et al., *Selective catalytic hydrogenation of nitriles to primary amines using iron pincer complexes.* Catalysis Science & Technology, 2016.

68. Xu, R., et al., *Iron-catalyzed homogeneous hydrogenation of alkenes under mild conditions by a stepwise, bifunctional mechanism.* ACS Catalysis, 2016. **6**(3): p. 2127-2135.

69. Frisch, M., et al., *Gaussian 09, rev.* B01,(Gaussian Inc., Wallingford CT, 2010), 2009.

70. Zhao, Y. and D.G. Truhlar, *A new local density functional for main-group thermochemistry, transition metal bonding, thermochemical kinetics, and noncovalent interactions.* The Journal of chemical physics, 2006. **125**(19): p. 194101.

71. Marenich, A.V., C.J. Cramer, and D.G. Truhlar, *Universal solvation model based on solute electron density and on a continuum model of the solvent defined by the bulk dielectric constant and atomic surface tensions.* The Journal of Physical Chemistry B, 2009. **113**(18): p. 6378-6396.

72. Chai, J.-D. and M. Head-Gordon, *Long-range corrected hybrid density functionals with damped atom–atom dispersion corrections.* Physical Chemistry Chemical Physics, 2008. **10**(44): p. 6615-6620.

73. Benitez, D., et al., *Experimentally-based recommendations of density functionals for predicting properties in mechanically interlocked molecules.* Journal of the American Chemical Society, 2008. **130**(45): p. 14928-14929.

74. Minenkov, Y., et al., *The accuracy of DFT-optimized geometries of functional transition metal compounds: a validation study of catalysts for olefin metathesis and other reactions in the homogeneous phase.* Dalton Transactions, 2012. **41**(18): p. 5526-5541.

75. Boonseng, S., et al., *The nature of the bonding in symmetrical pincer palladacycles.* Dalton Transactions, 2015. **44**(16): p. 7570-7577.

76. Gusev, D.G., *Assessing the accuracy of M06-L organometallic Thermochemistry.* Organometallics, 2013. **32**(15): p. 4239-4243.

77. Prokopchuk, D.E., et al., *Intramolecular C−H/O−H bond cleavage with water and alcohol using a phosphine-free ruthenium carbene NCN pincer complex.* Chemistry–A European Journal, 2014. **20**(51): p. 16960-16968.

78. Hehre, W. and L. Radom, *v. R. Schleyer, P.; Pople, JA Ab initio molecular orbital theory.* 1986, Wiley: New York.

79. Roddick, D.M., *Tuning of PCP pincer ligand electronic and steric properties*, in *Organometallic Pincer Chemistry.* 2013, Springer. p. 49-88.

80. Koehne, I., et al., *Synthesis and structure of six-coordinate iron borohydride complexes supported by PNP ligands.* Inorganic chemistry, 2014. **53**(4): p. 2133-2143.

81. Jiao, H., et al., *A comparative computationally study about the defined m (II) pincer hydrogenation catalysts (m= fe, ru, os).* Journal of computational chemistry, 2016. **37**(2): p. 168-176.

82. Grimme, S., et al., *A consistent and accurate ab initio parametrization of density functional dispersion correction (DFT-D) for the 94 elements H-Pu.* The Journal of chemical physics, 2010. **132**(15): p. 154104.

83. The small 6-31++(d,p) basis set used in geometry optimization affords DEPlx values that are very close to the ones obtained with the larger def2 basis set. This suggests the contribution from the basis set superposition error to be small in these energies.

84. Hasanayn, F. and R.H. Morris, *Symmetry aspects of H_2 splitting by five-coordinate d6 ruthenium amides, and calculations on acetophenone hydrogenation, ruthenium alkoxide formation, and subsequent hydrogenolysis in a model trans-Ru $(H)_2$(diamine)(diphosphine) system.* Inorganic chemistry, 2012. **51**(20): p. 10808-10818.

85. Dub, P.A. and T. Ikariya, *Quantum chemical calculations with the inclusion of nonspecific and specific solvation: Asymmetric transfer hydrogenation with bifunctional ruthenium catalysts.* Journal of the American Chemical Society, 2013. **135**(7): p. 2604-2619.

86. Bertini, F., et al., *Efficient and mild carbon dioxide hydrogenation to formate catalyzed by fe (ii) hydrido carbonyl complexes bearing 2, 6-(Diaminopyridyl) diphosphine pincer ligands.* ACS Catalysis, 2016. **6**(5): p. 2889-2893.

87. Bichler, B., et al., *Heterolytic cleavage of dihydrogen by an iron (II) PNP pincer complex via metal–ligand cooperation.* Organometallics, 2013. **32**(15): p. 4114-4121.

88. Lin, Z. and T.J. Marks, *Metal, bond energy, and ancillary ligand effects on actinide-carbon. sigma.-bond hydrogenolysis. A kinetic and mechanistic study.* Journal of the American Chemical Society, 1987. **109**(26): p. 7979-7985.

89. Morris, R.H., *Brønsted–Lowry Acid Strength of Metal Hydride and Dihydrogen Complexes.* Chemical reviews, 2016.

90. Wylie, W. and R.H. Morris, *Ester hydrogenation catalyzed by a ruthenium (II) complex bearing an N-heterocyclic carbene tethered with an "NH_2" group and a DFT study of the proposed bifunctional mechanism.* 2012.